RESEARCH ARTICLE

THE **FASEB** JOURNAL

Hypoxia compensates cell cycle arrest with progenitor differentiation during angiogenesis

Bárbara Acosta-Iborra[1] | **Maria Tiana**[1,2,3] | **Laura Maeso-Alonso**[4] |
Rosana Hernández-Sierra[1] | **Gonzalo Herranz**[1] | **Andrea Santamaria**[1] | **Carlos Rey**[1] |
Raquel Luna[1] | **Laura Puente-Santamaria**[1] | **Margarita M. Marques**[5] | **Maria C. Marin**[4] |
Luis del Peso[1,2,3] | **Benilde Jiménez**[1,2,3]

[1]Departamento de Bioquímica, Universidad Autónoma de Madrid (UAM), Instituto de Investigaciones Biomédicas "Alberto Sols" CSIC-UAM, Madrid, Spain

[2]IdiPaz, Instituto de Investigación Sanitaria del Hospital Universitario La Paz, Madrid, Spain

[3]CIBER de Enfermedades Respiratorias (CIBERES) Instituto de Salud Carlos III, Madrid, Spain

[4]Departamento de Biología Molecular, Laboratorio de Diferenciación Celular y Diseño de Modelos Celulares, Instituto de Biomedicina, Universidad de León, León, Spain

[5]Departamento de Producción Animal, Laboratorio de Diferenciación Celular y Diseño de Modelos Celulares, Instituto de Desarrollo Ganadero y Sanidad Animal, Universidad de León, León, Spain

Correspondence
Benilde Jiménez, Departamento de Bioquímica, Universidad Autónoma de Madrid (UAM), Instituto de Investigaciones Biomédicas "Alberto Sols" CSIC-UAM, C/Arturo Duperier 4. Madrid 28029, Spain.
Email: bjimenez@iib.uam.es

Present address
Maria Tiana, Centro Nacional de Investigaciones Cardiovasculares (CNIC), Madrid, Spain
Gonzalo Herranz and Carlos Rey, Centro de Biología Molecular Severo Ochoa CSIC-UAM, Madrid, Spain
Raquel Luna, Evotec (France) SAS, Toulouse cedex, France

Abstract
Angiogenesis, the main mechanism that allows vascular expansion for tissue regeneration or disease progression, is often triggered by an imbalance between oxygen consumption and demand. Here, by analyzing changes in the transcriptomic profile of endothelial cells (ECs) under hypoxia we uncovered that the repression of cell cycle entry and DNA replication stand as central responses in the early adaptation of ECs to low oxygen tension. Accordingly, hypoxia imposed a restriction in S-phase in ECs that is mediated by Hypoxia-Inducible Factors. Our results indicate that the induction of angiogenesis by hypoxia in Embryoid Bodies generated from murine Stem Cells is accomplished by the compensation of decreased S-phase entry in mature ECs and differentiation of progenitor cells. This conditioning most likely allows an optimum

Abbreviations: DE, differentially expressed; EBs, embryoid bodies; ECs, endothelial cells; EdU, 5-ethynyl-2′-deoxyuridine; GO, gene ontology; HUVEC, human umbilical vein endothelial cells; Hx, hypoxia; iPSCs, induced pluripotent stem cells; mESCs, mouse embryonic stem cells; MEFs, mouse embryonic fibroblasts; N, normoxia; 2D, two-dimensional; 3D, three-dimensional; 4sU, 4-thiouridine; PI, propidium iodide.

remoddeling of the vascular network. Identification of the molecular underpinnings of cell cycle arrest by hypoxia would be relevant for the design of improved strategies aimed to suppress angiogenesis in pathological contexts where hypoxia is a driver of neovascularization.

1 | INTRODUCTION

Complex organisms depend on oxidative metabolism to meet their energy requirements and therefore are strictly dependent on a constant oxygen supply. This explains why they are endowed with a molecular machinery specialized in sensing oxygen levels (Prolyl Hydroxylase Domain, PHDs) and coping with alterations in oxygen homeostasis. At the core of this machinery are the Hypoxia-Inducible Factors (HIFs), a family of heterodimeric transcription factors composed of alpha and beta subunits.[1] The stability and transcriptional activity of the HIFα subunit is regulated by oxygen levels, whereas the HIFβ subunit (Ah Receptor Nuclear Translocator, ARNT) remains unchanged. Of the three genes encoding for HIFα subunits, *HIF1A* and *EPAS1* (also known as *HIF2A*)[2-4] are the best-characterized members of the family. The proteins encoded by these genes share a common mechanism of regulation by hypoxia that involves the control of stability and transactivation activity through oxygen-dependent hydroxylation of specific residues.[5,6] However, these genes differ in their pattern of expression. While the *HIF1A* gene is ubiquitously expressed, *EPAS1* expression is restricted to specific tissues and cell types, being particularly abundant in ECs.[2,3,5] In addition, these factors regulate partially overlapping sets of target genes.[7,8]

Correlation between hypoxia (defined as an imbalance between oxygen supply and demand) and disease highlights the importance of oxygen homeostasis.[9] The HIF pathway is activated in a wide variety of pathological situations, including highly prevalent diseases such as cancer and cardiorespiratory diseases.[1,10,11] Thus, understanding how hypoxia regulates gene expression could open up new avenues for the clinical management of these diseases.

HIFs orchestrate a set of responses aimed to restore oxygen homeostasis by reducing metabolic oxygen consumption and increasing its delivery to hypoxic tissues. This latter effect is mediated by the induction of angiogenesis, which is the main mechanism for the formation of new vessels from pre-existing ones and a prototypical adaptive response to hypoxia. Deciphering the mechanisms involved in the induction of angiogenesis by hypoxia has been the subject of intensive research over the last decade,[12-15] but central aspects still remain to be understood. In particular, knowledge of the mechanisms controlling EC proliferation is scarce despite

its relevance for the formation of a fully functional vascular plexus. A proper control of EC division is paramount for the development of morphologically and functionally optimum vessels and excessive or scarce proliferation result in deleterious consequences. In this regard, excessive EC proliferation as a result of notch inhibition gives rise to increased microvascular density but defective perfusion in tumors[16] and mice lacking *Flt1* die of vascular overgrowth,[17] as a consequence of increased availability of VEGFA to bind to VEGFR2.[18] More recently, it has been demonstrated that an abnormally high mitogenic signal induced by the endothelial deletion of PTEN,[19] VEGFR2 gain-of-function or Notch loss-of-function[20] results in defective angiogenesis. Therefore, the mechanisms that ensure restriction of EC proliferation are fundamental; and a deep understanding of the pathways that fine-tune EC proliferation during the remodeling of the vasculature could be relevant for a successful therapeutic suppression or stimulation of angiogenesis in pathological contexts.

ECs are endowed with oxygen sensors (PHDs) and HIFs that allow them to mount adaptive responses to restore tissue oxygenation. Although seemingly counterintuitive, it is now widely accepted that ECs sense and respond to hypoxia by the activation of otherwise quiescent ECs (also called phalanx cells) to initiate a complex cascade of events that allows vessel growth.[13,21,22] Moreover, the autonomous response to hypoxia that occurs in *Drosophila* tracheal cells is a key step in tracheal sprouting,[22,23] suggesting that the activation of the HIF pathway within the luminal cells of oxygen-delivering structures may be an evolutionarily conserved process required for their sprouting toward hypoxic regions. New vessel formation requires the tight coordination of proliferation, differentiation, and migration. How hypoxia controls EC proliferation is poorly understood and constitutes the central aim of this study.

A transcriptomic study in Human Umbilical Vein Endothelial Cells (HUVEC) exposed to hypoxia allowed us to identify an early anti-proliferative gene expression signature. We functionally validated that hypoxia engages ECs in a slow proliferation mode, reducing the percentage of cells in the S-phase of the cell cycle. We demonstrated that HIF factors, and most prevalently EPAS1, are responsible for the decreased S-phase entry and proliferation rate of ECs under hypoxic conditions. This biological response required an

intact basic-Helix-Loop-Helix domain and therefore, HIF transcriptional activity. We further extended these results to a comprehensive in vitro model of angiogenesis based on the differentiation of Embryoid Bodies (EBs) generated from mouse Embryonic Stem Cells (mESCs). Our results showed that the induction of angiogenesis by hypoxia in the EB model is concomitant with a decreased S-phase entry in mature ECs that was balanced by the differentiation of progenitor cells.

2 | MATERIALS AND METHODS

2.1 | Cell culture and embryoid bodies

HUVEC from pools of donors were purchased from Lonza (Lonza, C2519A), grown in Endothelial Medium Bullet Kit (EGM-2, Lonza, CC-3162) and used from passage 5-7 for experiments. For viral production, HEK 293T was maintained in Dulbecco's modified Eagle's medium (Gibco, 41966052) supplemented with 50 U/mL of penicillin (Gibco, 15140122), 50 µg/mL of streptomycin (Gibco, 15140122), 2 mM glutamine (Gibco, 25030123) and 10% (v/v) fetal bovine serum (Gibco, 10270106). All cells were grown at 37°C and 5% CO_2 in a humidified incubator and tested regularly for mycoplasma contamination. For hypoxia treatment, cells were grown at 37°C in a 1% O_2, 5% CO_2, 94% N_2 gas mixture in a Whitley Hypoxystation H35 (Don Whitley Scientific). Murine 129 SvJ R1 wild-type mESCs (R1)[24] were a kind gift of Dr Lena Claesson Welsh (Uppsala University). E14TG2a[25] mESCs were kindly provided by Dr Maria C Marin. Murine-induced Pluripotent Stem Cells (iPSCs) were previously generated.[26] R1, E14TG2a, and iPSCs were cultured on a monolayer of mitomycin C (Sigma, M4287) inactivated Mouse Embryonic Fibroblasts (MEFs) in mESC medium (Dulbecco's modified Eagle's medium (Gibco, 41966052) supplemented with 50 U/mL of penicillin (Gibco, 15140122), 50 µg/mL of streptomycin (Gibco, 15140122), 2 mM GlutaMAX (Sigma, G8541), Non-Essential Amino acid Solution (Thermo Fisher Scientific, 11140050), 0.1 mM 2-mercaptoethanol (Thermo Fisher Scientific,21985023), 1000 unit/mL of ESGRO Leukemia Inhibitory Factor (LIF) (Chemicon, ESG1106) and 15% (v/v) fetal bovine serum pre-tested for mESC culture. Medium was changed every day and cells were split 1:10 every other day. For the generation of EBs, MEFs were separated from stem cells by differential binding to 1% gelatin in PBS for 30 minutes at 37°C. For EB formation, mESCs were aggregated in hanging drops (1200 cells/20 µL drop) and differentiated in mESC medium without LIF for 4 days. On Day 4, the R1-derived and E14TG2a-derived EBs were placed in 12 mm diameter coverslips in 24 well multiwell plates (1 EB/ well) or p100 culture plates (25 EBs/p100) coated with 1% gelatin in PBS for the two-dimensional differentiation of EBs (2D-EBs). 2D-EBs were transferred to hypoxia (1% oxygen) or maintained in normoxia (21% oxygen) for the last 48 hours or 72 hours of a total differentiation time of 10 days. The number of EBs per experimental condition was 18-29 EBs for R1-2D and 10 EBs for E14TG2a-2D. iPSC-derived EBs were differentiated in three dimensions (iPSC-3D-EBs) on collagen I. iPSC-EBs were flushed down from the lid with EB medium (DMEM/GlutaMAX (Thermo Fisher Scientific, 61965) supplemented with 25 mM HEPES (Thermo Fisher Scientific 15360), 1.2 mM sodium pyruvate (Thermo Fisher Scientific, 11360), 19 mM monothioglycerol (SIGMA, M6145) and 15% (v/v) fetal bovine serum), and embedded into a collagen I matrix (6 EBs/well in a 12-well plate) composed of Ham's F12 medium (PromoCell), 6.26 mM NaOH, 20 mM HEPES (Thermo Fisher Scientific, 15360), 0.117% $NaHCO_3$, 1% GlutaMAX I (Thermo Fisher Scientific, 35050) and 1.5 mg/ mL of collagen I (Advanced BioMatrix, 5005). The collagen matrix was covered with EB medium. EB medium was changed every 2 days. iPSC-3D-EBs were transferred to hypoxia (1% oxygen) or maintained in normoxia (21% oxygen) for the last 72 hours or 96 hours of a total differentiation time of 10 days. The number of EBs per experimental condition for iPSC-3D-EBs experiments was 12-21.

2.2 | Proliferation curves and cell viability

1.25×10^4 HUVEC were plated on 6-well multiwell plates and cultivated in normoxia (21% oxygen) or hypoxia (1% oxygen) for the indicated periods of time. HUVEC were dissociated to single cells by treatment with TrypLE-Express (Gibco, 12604-013), centrifuged at 500 g 7 minutes, resuspended in 170 µL of PBS containing 1 µg/mL of DAPI (Molecular Probes, D1306) or 2 µM TO-PRO-3 Iodide (Molecular Probes, T3605) (for cell viability quantification) and counted by flow cytometry using Perfect Counts microspheres (Cytognos, CYT-PCM-50) (30 µL per experimental condition). Sample measurements were performed with BD FACSDIVA Software (Version 6.2, BD Biosciences). Data analysis was performed following Perfect Counts microspheres instructions. Linear regression analysis was performed according to the following equation:

$$\log_2 N_t = \log_2 N_0 + \frac{1}{T}t$$

t (time hours), N_t (cell number at time t), N_0 (initial cell number), and T (doubling time).

2.3 | EdU incorporation and quantification by microscopy and flow cytometry

Detection of EdU (5-ethynyl-2′-deoxyuridine) by microscopy in HUVEC and EBs was performed by Click-iT EdU

Alexa Fluor 647 Imaging Kit (Thermo-Fisher Scientific, C10340) according to the manufacturer's instructions. 2×10^4 HUVEC were grown on 12 mm diameter coverslips in 24 well multiwell plates in normoxia or hypoxia for the indicated periods of time and 10 µM EdU was added during the last 3 hours. Cells were fixed with 3.7% paraformaldehyde in PBS 20 minutes at room temperature (RT) and incubated with 0.1 M glycine in PBS 20 minutes, followed by PBS washing and storage at 4°C in PBS or at −20°C in 70% ethanol until processing following Click-iT instructions. Images of HUVEC were acquired with a 10X objective (Plan-Fluor 10×/0.3) using a fluorescence microscope Eclipse 90i (Nikon) and analyzed with ImageJ software (https://imagej.nih.gov/ij/).[27] Quantification of the percentage of S-phase cells in HUVEC was performed in binary images by automatic counting using the ImageJ command analyze particles. EBs were generated and differentiated as indicated in the previous section and 10 µM EdU was added during the last 3 hours. For 2D-EBs experiments, images of 4-15 fields of peripheral and internal vascular structures per EB were acquired with a 25X objective (Plan-Apochromat 25×/0.8 Imm Korr DIC) using a LSM710 confocal microscope (Zeiss) for each experimental condition. To quantify the percentage of S-phase cells in vascular structures in 2D-EBs we designed a semi-automatic macro (Supplemental Figure S1A-C) that allowed the automatic counting of ERG positive nuclei in CD31 positive endothelial cells (CD31$^+$ ERG$^+$ mask), followed by manual counting of EdU positive endothelial cell nuclei in the maximum intensity Z-projection using the cell counter plugin of ImageJ after the visual validation of endothelial identity synchronizing the maximum intensity Z-projection with the Z-stack (Supplemental Figure S1A-C). For 3D-EBs experiments, images of the EBs were acquired with a 25X objective (LD LCI Plan-Apochromat 25×/0.8 Imm Korr DIC M27) using a LSM800 confocal microscope (Zeiss) for each experimental condition. The quantification of the percentage S-phase cells in vascular structures in 3D-EBs was performed in binary images of maximum intensity Z-projections by automatic counting using the ImageJ command analyze particles (Supplemental Figure S1D). For flow cytometry analysis, 2×10^5 HUVEC were grown in p60 dish and cultured in normoxia or hypoxia for the indicated periods of time and 10 µM EdU was added during the last hour. Cells were centrifuged at 500 g 7 minutes, the pellet was resuspended by vortexing, cells were fixed in 0.5 mL of 70% ethanol and incubated 20 minutes at 4°C before storing at −20°C until processing by Click-iT. Click-iT detection was performed as follows: cells were centrifuged at 500 g 7 minutes, washed with 1 mL of 0.1% Tween-20 (Sigma, P9416) in PBS, resuspended in 50 µL of freshly prepared EdU detection reaction buffer (PBS, 2 mM CuSO$_4$ (Sigma, C7631), 0.05 mM Biotin Azide (Molecular Probes, B10184), 5 mM ascorbic acid (Sigma, A-4544)), and incubated 30 minutes at RT

protected from light. After washing with 0.1% Tween-20 in PBS, cells were resuspended in 50 µL of Streptavidin-AF647 (Molecular Probes, B10184) diluted 1:200 in PBS containing 0.1% Tween-20 and 3% BSA (NZYTech, MB04602) and incubated 30 minutes at RT protected from light. Cells were washed with 1 mL of 0.1% Tween-20 in PBS, centrifuged and resuspended in 200 µL of PBS containing 250 µg/mL of RNase and 10 µg/mL of propidium iodide (PI) (Cell Signaling Technology, 4087S) or 1 µg/mL of 4′,6-diamidino-2-phenylindol (DAPI Molecular Probes, D1306) followed by an incubation at RT protected from light. For flow cytometry analysis in EBs, 50 EBs per experimental condition (25 EBs/p100) were used and 10 µM EdU was incorporated during the last hour. EBs were dissociated to single cells by treatment with 1 mg/mL of Dispase II (Roche, 04 942 078 001) in PBS, 20 minutes at 37°C, followed by 2 min incubation with 1 mL of cell dissociation solution non-enzymatic (Sigma, C5914) and mechanical dissociation by pipetting. Cells were centrifuged at 500 g 7 minutes and counted using a Neubauer chamber (Hausser Scientific, 1492). 10^6 cells were resuspended in 50 µL of PBS, fixed with 1ml of 70% ethanol and incubated 20 minutes at 4°C before storing at −20°C for staining. Click-iT detection was performed as indicated above. After the Click-iT reaction, cells were resuspended in 100 µL of 3% BSA in PBS and 1 µg of anti-VE-Cadherin-PE antibody (BD Biosciences, 560410) or isotype control antibody was added and incubated 40 minutes at 4°C protected from light. After washing with 3 mL of PBS, cells were centrifuged at 500 g 5 minutes and resuspended in 200 µL of PBS containing 1 µg/mL of DAPI. Flow cytometry was performed in a three laser (405nm, 488 nm, 633 nm) flow cytometer (FACScantoII BD Biosciences). EdU-Alexa 647 was measured upon excitation with the 633 nm laser using a 660/20 band-pass filter. A minimum of 10^4 events was acquired per experimental condition in slow rate mode to avoid doublets. Sample measurements were performed with BD FACSDIVA Software (Version 6.2, BD Biosciences). Data analysis was performed with FlowJo 9/10 Software (Ashland). Cell debris and aggregates were excluded from the analysis using pulse processing FSC-A vs SSC-A, FSC-A vs FSC-H, and Pacific Blue-A vs Pacific Blue-H when appropriate. Cells co-stained with EdU-Alexa 647 and PI or DAPI were used to measure the percentage of cells in G_0/G_1, S, and G_2/M phases of the cell cycle.

2.4 | Immunofluorescence staining

For immunofluorescence staining, HUVEC growing on coverslips or 2D-EBs attached to coverslips coated with 1% gelatin in PBS were fixed in 3.7% paraformaldehyde in PBS for 20 minutes at room temperature and incubated with 0.1 M glycine in PBS for 20 minutes, followed by PBS washing

and storage at 4°C in PBS or at −20°C in 70% ethanol until processing for detection with antibodies. Fixed cells or 2D-EBs were permeabilized with 0.5% Triton X-100 in PBS for 20 minutes, washed with PBS and blocked with 3% BSA in PBS for 20 minutes at room temperature. Antibodies used for immunofluorescence were diluted in PBS containing 3% BSA and 0.1% Tween-20 as follows: 1:500 mouse anti-HIF1α (BD Biosciences, 610 959), 1:100 rabbit anti-EPAS1 (Novus, NB100-122), 1:1000 rat anti-mouse CD31 (BD Biosciences, BD#553370), 1:1000 rabbit anti-ERG (Abcam, ab92513), 1:500 Alexa Fluor 488 goat anti-mouse (Molecular Probes, A11029), 1:500 Alexa Fluor 546 goat anti-rabbit (Molecular Probes, A11035), 1:500 Alexa Fluor 546 goat anti-rat (Molecular Probes, A11081), and 1:500 Alexa Fluor 488 donkey anti-rabbit (Molecular Probes, A21206). Primary antibodies were incubated overnight at 4°C and secondary antibodies 1 hour at room temperature in a humidified chamber. Washings after incubation with primary and secondary antibodies (3 × 10 minutes for HUVEC and 4 × 40 minutes for EBs) were performed with 0.1% Tween-20 in PBS at room temperature. After immunostaining, DNA was stained with 1.25 µg/mL of DAPI (Molecular Probes, D1306) in PBS for nuclei visualization. Coverslips were mounted on slides with Prolong (Molecular Probes, P36970) as an antifading reagent. For IB4 detection, 3D-EBs embedded in collagen I were washed twice with PBLEC buffer (0.1 mM CaCl2, 0.1 mM MnCl2, 0.1 mM MgCl2, 1% Triton-X 100 in PBS pH 6.8) followed by incubation with 1 µg/mL of biotinylated isolectin B4 (Sigma, L2140) in PBLEC, at 4°C overnight. EBs were washed three times with 0.05% Tween-20 in PBS (1 hour per wash) and then incubated with 1 µg/mL of Steptavidin-Alexa555 (Invitrogen, S32355) in PBS containing 3% BSA and 0.1% Tween-20 for 1 hour at RT. Three additional washes were performed with 0.05% Tween-20 in PBS. After immunostaining, DNA was stained with 1 µg/mL of DAPI for nuclei visualization, before mounting the EBs with Fluoromount-G (Aname, 17984-25).

2.5 | Confocal microscopy and quantification of angiogenesis

Images of 4-15 fields per EB of peripheral and internal vascular structures of the 2D-EBs were acquired with a 25X objective using a LSM710 confocal inverted microscope (Zeiss) with laser lines 405, 488, 561, and 633 nm for each experimental condition. Images of the 2D-EBs were acquired using the *tile* tool of a LSM710 confocal microscope (Zeiss) with a 10× objective (Plan-Apochromat 10×/0.45 DIC) and images of the 3D-EBs were acquired using the *tile* tool of a LSM 800 confocal microscope (Zeiss) with a 25X objective (LD LCI Plan-Apochromat 25×/0.8 Imm Korr DIC M27). For quantitative analysis of angiogenesis in the EB model,

we used the AngioTool software (https://ccrod.cancer.gov/confluence/display/ROB2/Home), which allows to quantify several parameters related to vascular networks such as the area covered by a vascular network (total explant area), total vessel length, lacunarity, branching index, and end points index.[28] Non-structured areas (usually in the center of the EB) were cropped using the ImageJ tool prior to analysis by the AngioTool. For the generation of the AngioTool skeleton of the complex vascular structures in 2D-EBs and 3D-EBs, tools were selected in the indicated range: vessel diameter (1-8), vessel intensity (0-255), remove small particles (50-300), and fill holes tool was adjusted to 50 (Supplemental Figure S1E,F).

2.6 | Functional enrichment analysis and clustering analysis

Gene expression profiles of HUVEC (GEO accession GSE89831) were analyzed with the Bioconductor's[29] edgeR package[30] for the R statistical software (http://www.R-project.org/), to identify genes whose transcription was affected by hypoxia. Specifically, we considered differentially expressed (DE) genes those whose expression in the 4-thiouridine (4sU)-labeled fraction, used as a proxy for transcription rate,[31] was significantly different in the normoxic and hypoxic samples (FDR-adjusted *P*-value < .05) and the absolute change in expression was at least 2-fold:

$$\left| \log_2\left(\frac{H_i}{N_i}\right) \right| \geq 1.$$

where H_i and N_i represent the expression of gene i under hypoxia and normoxia, respectively. Then, we performed an enrichment test for Gene Ontology (GO) terms based on hypergeometric distribution with the clusterProfiler[32] and represented the enrichment results using the functions in the enrichplot package.

2.7 | Western blot

Cells were lysed in RIPA buffer (50 mM Tris-HCl pH 8, 150 mM NaCl, 0.02% NaN₃, 0.1% SDS, 1% NP-40, containing protease inhibitors (Complete ULTRA table, Roche, 06538304001). Protein concentration was quantified using Bio-Rad DC protein assay (Bio-Rad, 5000112) and 20 µg of each sample was resolved in 10% SDS-polyacrylamide gels. Proteins were transferred to the polyvinylidene difluoride (PVDF) membrane (Immobilon-P, Millipore, IPVH100010). Membranes were blocked with 5% non-fat dry milk in TBS-T (50 mM Tris-HCl pH 7.6,

150 mM NaCl, 0.1% Tween-20) and incubated with the corresponding antibodies: mouse anti-HIF1α (1:1000; BD Biosciences, 610959), rabbit anti-EPAS1 (1:1000; Novus, NB100-122), mouse anti-Tubulin (1:2000; Sigma, T6199), Goat Anti-Mouse-HPR (1:5000; Promega, W402B), and Goat Anti-Rabbit-HPR (1:5000; MP Biomedicals, 855690). Washings after antibody incubations were performed in TBS-T. Western-blots were developed by enhanced chemiluminescence (Clarity western ECL substrate Bio-Rad, 170-5060).

2.8 | RNA extraction and qRT-PCR

RNA was extracted and purified using the RNeasy Mini Kit (Qiagen, 74106) following the manufacturer's instructions. For quantitative-RT PCR analysis 1 μg of total RNA of each sample was reversed-transcribed to cDNA (Transcriptor First Strand cDNA Synthesis kit, Roche, 04379012001), cDNA was diluted 1:20 and used as a template for amplification reactions, carried out with the Power SYBR Green PCR Master Mix (Applied Biosystems, 4367659) or TaqMan Universal Master Mix II (Applied Biosystems, 4440040), following manufacturer's instructions. PCR amplifications were carried out in a StepOne Real-time PCR System (Applied Biosystems, 4376357). Data were analyzed with StepOne software and expression levels were calculated using ΔΔCT, using β-actin as reference. The following primers sequences were used for qRT-PCR analysis: *ACTB* (forward 5′ AAGGCCAACCGCGAGAAG 3′; reverse 5′ ACAGCCTGGATAGCAACGTAC 3′), *EGLN3* (forward 5′ ACACGAAGTGCAGCCCTCTT 3′; reverse 5′ TCTTCAGCATCAAAGTACCAGACAGT 3′), *VEGFA* (forward 5′ CCTTGCTGCTCTACCTCCAC 3′; reverse 5′ ATGATTCTGCCCTCCTCCTT 3′), *ODC1* (forward 5′ TTCCAGAGGCCGACGATCTA 3′; reverse 5′ TGGCGTTTCATCCCACTCTC 3′), *ANGPTL4* (forward 5′ CACCTAGACCATGAGGTGGC 3′; reverse 5′ GACCCCTGAGGCTGGATTTC 3′), *BNIP3* (forward 5′ GGTCAAGTCGGCCGGAAAAT 3′; reverse 5′ TGGAGGTTGTCAGACGCCTT 3′)*E2F1* (forward 5′ TCCAGCTCATTGCCAAGAAGT 3′; reverse 5′ CTGGGTCAACCCCTCAAGC 3′), *E2F2* (forward 5′ CAAGTTGTGCGATGCCTGCC 3′; reverse 5′ TTGGGAACTCAGGGACGACG 3″), *E2F8* (forward 5′ CCTTGGCACCTTGAAGAGCA 3′; reverse 5′ CTGCCCGAAATTCCACTCCA 3′), *CCND1* (forward 5′ TGCTGCGAAGTGGAAACCATC 3′; reverse 5′ CACTTCTGTTCCTCGCAGAC 3′), *CCNE1* (forward 5′ CAGGGAGCGGGATGCG 3′; reverse 5′ GGGTCTGCACAGACTGCAT), *HIF1A* (Applied Biosystems, TaqMan probe HS00936368_m1) and *EPAS1* (Applied Biosystems, TaqMan probe HS01026149_m1).

2.9 | Lentiviral production

Lentiviral vector pGIPZ was used for the expression of shRNAs to specifically silence *HIF1A* (V2LHS_132150) or *EPAS1* (V2LHS_113753) (Open Biosystems). A scramble, non-silencing shRNA was used as control (Open Biosystems, NS; RHS4346). *HIF1A* and *EPAS1* mutants were cloned using In-Fusion HD Cloning Kit (Takara, 639689) in pRRL-IRES-EGFP vector[33] using the same constructs as in Kondo et al.[34] ODD proline residues were converted to alanine for maintaining HIF constitutively active in normoxic conditions (pRRL-HIF1α-P402A; P564A-IRES-EGFP and pRRL-EPAS1-P405A; P531A-IRES-EGFP). Additionally, we used double mutants in which the bHLH motif had been mutated to prevent DNA-binding (pRRL-HIF1α-P402A; P564A-bHLH*-IRES-EGFP and pRRL-EPAS1-P405A; P531A-bHLH*-IRES-EGFP). All vectors were confirmed by DNA sequencing. Lentivirus was produced and titrated in HEK 293T cells as previously described.[33] For the transduction of HUVEC, lentiviruses were used at a multiplicity of infection (MOI) of 1-2 for 8 hours, resulting in more than 95% transduced (EGFP-positive) cells 72 hours after infection.

2.10 | Statistical analysis

GraphPad Prism version 5.03 for Windows (GraphPad Software, La Jolla, CA, USA) was used for statistical analysis. Data were reported as the mean and $P < .05$ was considered significant.

3 | RESULTS

3.1 | Identification of an anti-proliferative gene expression signature imposed in endothelial cells by hypoxia

To cope with fluctuations in oxygen levels eukaryotic cells undergo an extensive gene expression reprogramming, mainly driven by HIFs, that have been studied in different cell types and biological contexts.[35,36] Herein, we aimed to identify biological functions enriched in genes whose transcription is regulated by oxygen levels in ECs to get further insight into one of the central adaptive responses to hypoxia. To this end, we exposed HUVEC to hypoxia (1% O_2) or normoxia (21% O_2) for 8 hours and pulse-labeled them with 4sU to label nascent RNA and then characterized the pattern of newly transcribed mRNAs by affinity capture of the labeled transcripts followed by high-throughput sequencing.[31] Differential expression analysis identified 196 genes whose transcription was robustly induced by hypoxia ($log_2FC>=1$ and FDR $< .05$) and 201 genes strongly

repressed ($\log_2 FC <= -1$ and FDR < .05). We performed a Gene Ontology (GO) enrichment analysis on the data from this experiment and found that several biological categories related to response to hypoxia, vascular development, and angiogenesis were significantly overrepresented in the genes upregulated by hypoxia in HUVEC (Figure 1). Unexpectedly, we also found that categories related to cell cycle regulation and DNA replication were significantly enriched in the genes downregulated by 8 hours hypoxia in HUVEC. Figure 1A shows the clustering of the main GO terms enriched in genes differentially expressed in hypoxic cells compared to control cells, highlighting the predominance of repression of the cell cycle, together with angiogenesis, as the biological responses in the early adaption of HUVEC to low oxygen tension. Figure 1B graphically depicts that 38 out of a total of 201 genes transcriptionally repressed by hypoxia in HUVEC had GO annotations related to DNA replication or cell cycle G1/S phase transition. The data of the top six GO categories enriched in the set of genes DE shown in Figure 1B are included in Supplemental Table 1. It is worth mentioning that the category related to DNA replication includes 40 genes and 38 of them (95%) were downregulated by hypoxia in HUVEC. In agreement, a large number of critical regulators of the central pathways controlling G1/S transition and DNA replication were negatively regulated by hypoxia in HUVEC (Figure 1C). This early anti-proliferative gene expression signature imposed by hypoxia in HUVEC was maintained up to the later time point analyzed (16 hours, data not shown). Figure 1D shows the validation by qRT-PCR of decreased expression by hypoxia of a representative set of genes related to G1/S transition of the cell.

Thus, our transcriptomic analysis unveiled that in contrast to the more intuitive view, hypoxia most likely arrests the EC division cycle.

3.2 | Hypoxia decreases the percentage of endothelial cells in the S-phase of the cell cycle

Since the anti-proliferative gene expression signature inferred from the RNA-Seq experiments in HUVEC is seemingly in conflict with the angiogenesis mechanism, we functionally validated this result by analyzing the effect of hypoxia in the percentage of HUVEC in the S-phase of the cell cycle. Exponentially growing asynchronous HUVEC were exposed to normoxia or hypoxia for 24 hours, 48 hours or 72 hours and briefly pulsed with the thymidine analog EdU to mark cells traversing S-phase. The percentage of HUVEC in S-phase quantified by microscopy (Figure 2A,B) was significantly lower in cells growing in hypoxia (24 hours Hx 21.3% ± 11.2% vs N 44.7% ± 8.9%; 48 hours Hx 2.9% ± 2.1%, vs N 28.4% ± 10.3%) (Figure 2B). Analysis by flow cytometry confirmed the reduction in the percentage of HUVEC in

S-phase in hypoxia compared to normoxia. (48 hours hypoxia 20 ± 8.4% vs normoxia 36.3% ± 3.2%; 72 hours hypoxia 10.6% ± 3.9% vs normoxia 31.6% ± 2.7%) (Figure 2C,D). In addition, hypoxia significantly increased the percentage of HUVEC in G_0/G_1 phase (48 hours hypoxia 61.8% ± 11.5% vs normoxia 44.5% ± 3.1%; 72 hours hypoxia 72.6% ± 7.5% vs normoxia 50.4% ± 1.2%) (Figure 2D).

In agreement with these observations, hypoxia reduced the cell proliferation rate of HUVEC (Figure 2E). Linear regression analysis with logarithmic transformation of the proliferation curves (Figure 2F), showed a significant reduction of the doubling time of HUVEC in hypoxia (hypoxia 47.96 ± 10.44 hours vs normoxia 20.4 ± 1.37 hours). We confirmed by DAPI or TO-PRO-3 staining that alterations in the cell cycle were not an indirect consequence of reduced viability, but a direct result from the attenuated proliferation of HUVEC in low oxygen tension (data not shown).

These data indicate that the adaptation of ECs to hypoxic conditions implies an adjustment of the cell cycle kinetics and in particular a decreased rate of S-phase entry.

3.3 | HIFs mediate the decreased proliferation rate of endothelial cells in hypoxia through a mechanism involving the basic Helix-Loop-Helix transcriptional domain

As a large number of the adaptive responses to hypoxia are mediated by the Hypoxia-Inducible Factors (HIFs), we sought to explore whether a decreased rate of S-phase entry imposed by hypoxia in ECs was mediated by these factors.

To this end, we generated lentiviral constructs to constitutively express active forms of EPAS1 or HIF1α in which the oxygen-sensitive proline residues were substituted by alanine to prevent their hydroxylation (pRRL-EPAS1PP, pRRL-HIF1αPP); rendering these mutants constitutively active in normoxia. Additionally, we generated double mutants in which the basic Helix-Loop-Helix (bHLH) transcriptional domain was altered to prevent binding to DNA (pRRL-EPAS1PPbHLH*, pRRL-HIF1αPPbHLH*). Supplemental Figure S2A,B shows the protein expression levels of these mutants by western-blot and immunofluorescence 48 hours after lentiviral transduction of HUVEC in normoxic conditions. We functionally validated the activity of these HIF mutants by analyzing the expression levels of preferential target genes for EPAS1 (*ANGPTL4*) or HIF1A (*EGLN3*) by qRT-PCR. Supplemental Figure S2C,D shows that, both EPAS1PP and HIF1αPP induced *VEGFA*, while HIF1αPP induced *EGLN3* and EPAS1PP induced *ANGPTL4* and repressed *ODC1*. None of the HIF-targets analyzed were regulated by the double mutants lacking a functional DNA binding domain (EPAS1PPbHLH*, HIF1αPPbHLH*).

We next used these gain of function mutants (EPAS1PP and HIF1αPP) and loss of function mutants (EPAS1PPbHLH*, HIF1αPPbHLH*) as a genetic approach to address whether HIFs were directly mediating the decreased S-phase entry observed in HUVEC growing in hypoxic conditions. The expression of constitutively active EPAS1 (EPAS1PP) in normoxia reduced the percentage of S-phase cells quantified by microscopy (pRRL-EPAS1PP 10.8% ± 1.6% vs pRRL 32.3% ± 1.4%) (Figure 3A,B). Likewise, expression of stabilized HIF1-alpha (HIF1αPP) in normoxia also had a significant effect over control although of smaller magnitude (N pRRL-HIF1αPP 20.5% ± 2.8% vs N pRRL 32.3% ± 1.4%).

(A)

(B)

(C)

(D)

FIGURE 1 Identification of an anti-proliferative gene expression signature imposed by hypoxia in endothelial cells. The effect of 8 hours hypoxia on HUVEC transcription was determined from the sequencing of the 4sU-labeled mRNA fraction (GEO accession GSE89831). We considered differentially expressed (DE) genes, those whose transcription was significantly (FDR < .05) and robustly (absolute change in the transcription of at least 2-fold) affected by hypoxia. A, DE genes were used as input for a GO enrichment analysis and the 16 top scoring categories represented into a network with edges connecting overlapping gene sets. Nodes in the graph represent the GO terms enriched in the list of DE genes. The color code of the nodes indicates the *P*-value for the association of each GO-term with the DE genes and the size of the nodes the number of genes in the category. The edges connect overlapping GO terms and the thickness of the edge the magnitude of overlap. B, Heatmap representing the effect of hypoxia on the transcription of DE genes belonging to the indicated GO categories. Horizontal lines represent individual DE genes and the color code the log-fold change in transcription, with red hues representing genes upregulated in hypoxia and blue hues genes repressed under hypoxia. The data of the top six GO categories enriched in the set of genes DE shown in Figure 1B are included in Supplemental Table 1. C, The Kyoto Encyclopedia of Genes and Genomes (KEGG) graph of the human Cell Cycle pathway (pathway ID hsa04110) is shown. Genes are colored according to their log-fold change in response to hypoxia as indicated by the legend. D, The effect of hypoxia on the expression of a representative set of genes related to G1/S control was determined by qRT-PCR in HUVEC treated 8 hours, 16 hours and 24 hours in hypoxia or normoxia. The graph represents the log2 ratio of hypoxia over normoxia determined in three independent experiments (each symbol represents an independent experiment). Statistical significance was determined by two-way ANOVA using Tukey's post-test (*$P < .05$, **$P < .01$, ****$P < .0001$)

Abrogation of the DNA binding capability of EPAS1PP and HIF1αPP prevented their impact on S-phase entry in HUVEC (N pRRL-EPAS1PPbHLH* 35.7% ± 7.9% and N pRRL-HIF1αPPbHLH* 38.8% ± 5.2%).

These results were further confirmed by flow cytometry analysis (Figure 3C,D). EPAS1PP decreased the percentage of HUVEC in S-phase (N pRRL-EPAS1PP 3.7% ± 1.2% vs N pRRL 23.8% ± 7.4%) and this effect was not observed when HUVEC were transduced with the double EPAS1PPbHLH* mutants lacking DNA binding capability (N pRRL-EPAS1PPbHLH* 22.9% ± 8%). We observed a similar trend as described for microscopy analysis with HIF1αPP and HIF1αPPbHLH* mutants, but in the analysis by flow cytometry differences from control did not reach statistical significance.

An analysis of the distribution of HUVEC in the cell cycle phases showed that the expression of EPAS1PP but not HIF1αPP increased the percentage of cells in the G_0/G_1 phase (N pRRL-EPAS1PP 81.9% ± 7.6% and N pRRL-HIF1αPP 68.3% ± 9.6% vs N pRRL 63.3% ± 10.8%) (Figure 3D). These results were in agreement with our transcriptomic study (Figure 1C). Changes induced by EPAS1PP in the cell cycle distribution were dependent on the presence of an intact bHLH domain, as the cell cycle distribution observed with the double mutants EPAS1PPbHLH* was similar to the one observed in control cells (Figure 3D).

Additionally, down-regulation of mRNA expression of *E2F1*, *E2F2*, *CCND1*, and *CCNE1* was mainly induced by EPAS1 and required an intact bHLH domain (Supplemental Figure S2E).

We next investigated the requirement of HIF for the effect of hypoxia on cell cycle using a loss of function approach based on interference by lentiviral transduction of shRNAs specific to *EPAS1* (pGIPZ-shEPAS1) or *HIF1A* (pGIPZ-shHIF1α); compared to scramble non-interference shRNAs (pGIPZ-shScr). Figure 4A-C shows the validation of the interference strategy. Increased G_0/G_1 and decreased S-phase induced by hypoxic conditions in HUVEC was abrogated by the interference of *EPAS1* (Figure 4D-G). However, the effect of *HIF1A* interference reached statistical significance by microscopy (Figure 4D,E), but not by flow cytometry (Figure 4F,G) analysis.

Taken together these results demonstrate that among HIFs, specifically the EPAS1 isoform, is predominantly involved in the regulation of the cell cycle of ECs to cope with reduced oxygen availability. Additionally, decreased S-phase entry induced by HIF required an intact bHLH domain and is, therefore, dependent on the transcriptional activity of HIF.

3.4 | Hypoxia decreases the percentage of S-phase mature endothelial cells in vascular structures in embryoid bodies generated from mouse embryonic stem cells

We next investigated whether cell cycle arrest occurred during vessel sprouting induced by hypoxic conditions. To this end we used Embryoid Bodies (EBs) generated from mouse Embryonic Stem Cells (mESC); a high-quality model for vascular development that faithfully recapitulates vasculogenesis (vessel formation from endothelial progenitor cells) and angiogenesis (sprouting of vascular structures).[37]Given that hypoxia is a potent inducer of EC differentiation in the early stages of EB formation,[38,39] we decided to interrogate the effect of low oxygen tension in S-phase entry of mature ECs in organized vascular structures. EBs generated from R1 mESCs were incubated in hypoxic or normoxic conditions for the last 48 or 72 hours of 10 days of differentiation in two dimensions (R1-2D-EBs) (Figure 5A). Figure 5B,C shows that hypoxic conditions increased the complexity of the vascular structures assembled in the EBs and significantly augmented the percentage of EBs with high angiogenesis score
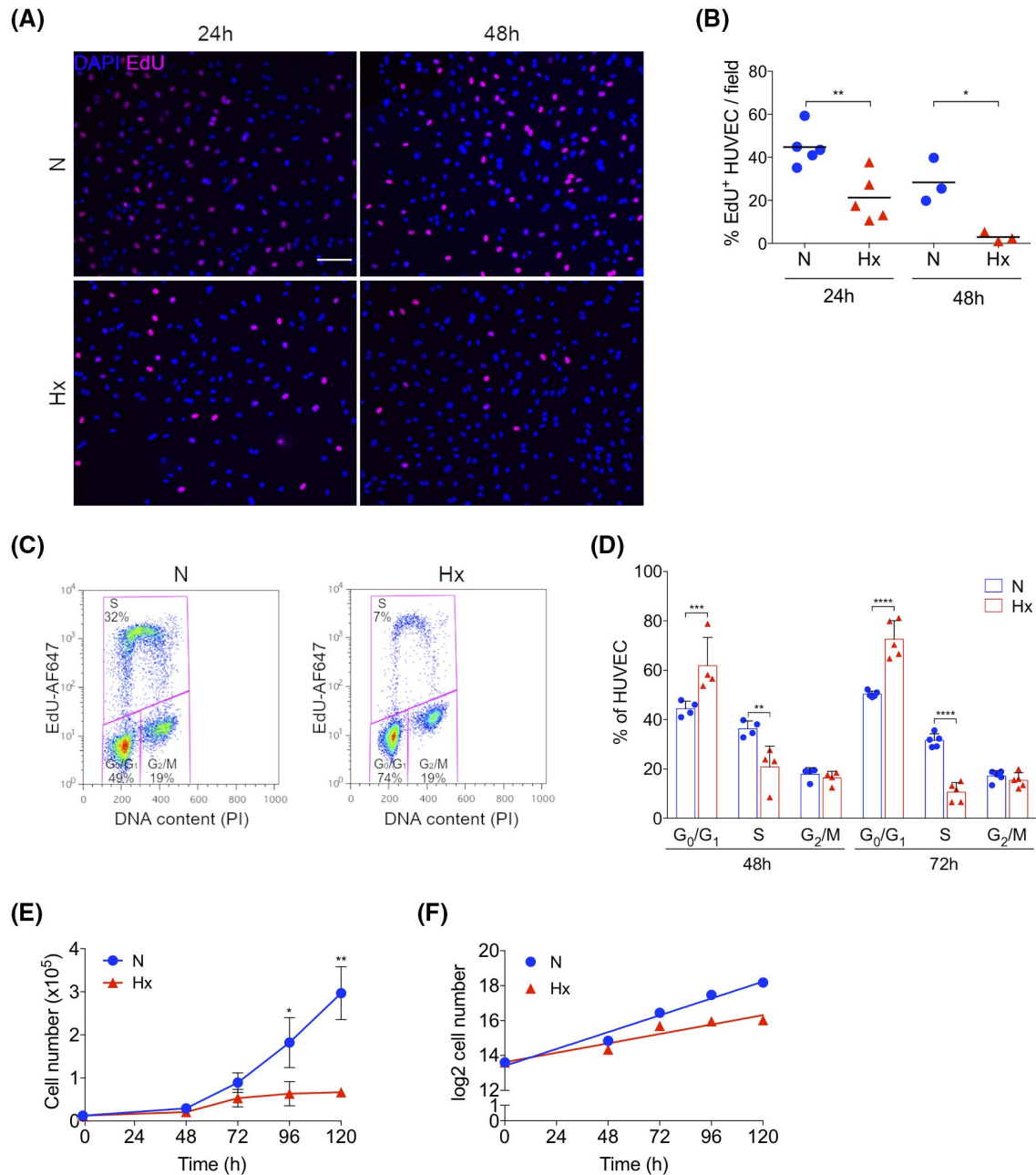
FIGURE 2 Hypoxia decreases the percentage of endothelial cells in the S-phase of the cell cycle. Exponentially growing asynchronous HUVEC were exposed to 21% oxygen (N) or 1% oxygen (Hx) and the cells were pulse labeled with EdU to quantify the percentage of S-phase cells by microscopy (A and B) or flow cytometry (C and D), respectively. A, A Representative microscopy image of each experimental condition (24 hours or 48 hours N or Hx) is shown. EdU$^+$ nuclei are shown in magenta and nuclei were visualized by DAPI staining. Bar: 100 μm. B, Percentage of EdU$^+$ cells/field in N (blue circles) or Hx (red triangles) in 3-5 independent experiments (10 fields were quantified per experimental condition and each symbol corresponds to the mean value of one experiment). Statistical significance was determined by one-way ANOVA using Tukey's post-test (*$P < .05$, **$P < .01$). C, Representative plot of EdU-Alexa 647 vs DNA content by propidium iodide staining (PI) of each experimental condition (72 hours N or Hx) is shown. Percentage of cells in G_0/G_1, S, and G_2/M phases of the cell cycle is shown inside the corresponding gating regions (magenta lines). D, Percentage of cells in G_0/G_1, S, and G_2/M phases quantified by FACS in N (blue circles) or Hx (red triangles). Symbols correspond to the value of independent experiments and bars represent the mean of 4-5 independent experiments. Statistical significance was determined by two-way ANOVA using Sidak's post-test (**$P < .01$, ***$P < .001$, ****$P < .0001$). E, Cell proliferation curves in N (blue circles) or Hx (red triangles). Cell number was quantified by flow cytometry using perfect count microspheres. Each point represents the mean of three independent experiments. Statistical significance was determined by two-way ANOVA using Sidak's post-test (*$P < .05$, **$P < .01$). F, Linear regression analysis of proliferation curves. The doubling time was significantly reduced in hypoxia compared to normoxia (Single sample paired Student's t-test, $P < .05$)
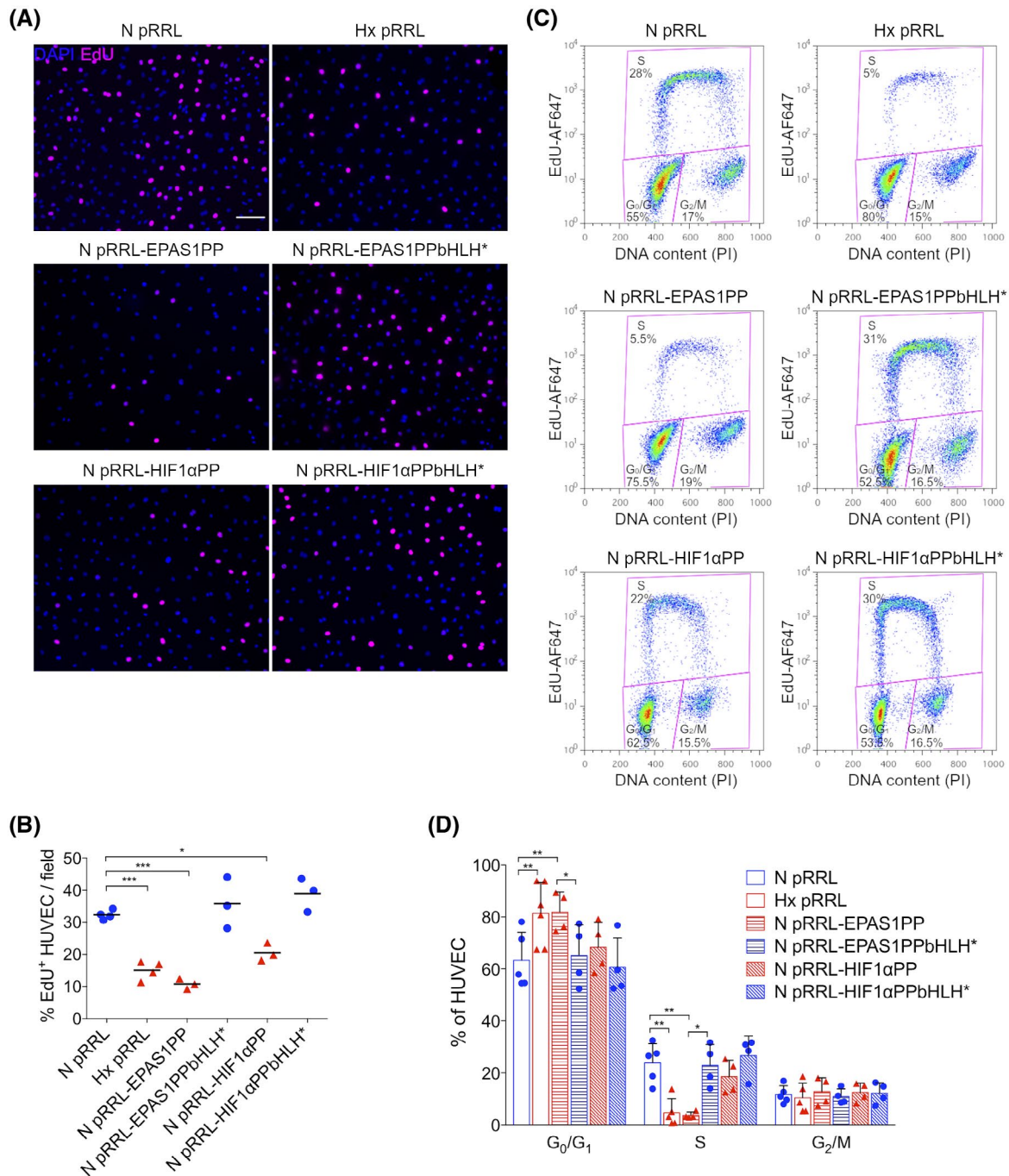
FIGURE 3 HIF mutants stabilized in normoxia decrease the percentage of endothelial cells in the S-phase of the cell cycle. Exponentially growing asynchronous HUVEC were infected with control lentivirus (pRRL), lentivirus for the expression of EPAS1 or HIF1A mutants stabilized in normoxia (pRRL-EPAS1PP, pRRL-HIF1αPP), or lentivirus for the expression of double mutants whose bHLH domain has also been mutated (pRRL-EPAS1PPbHLH*, pRRL-HIF1αPPbHLH*). Transduced HUVEC were pulse labeled with EdU to quantify the percentage of S-phase cells by microscopy (A-B) or flow cytometry (C-D) 48 hours after infection. A, A representative microscopy image of each experimental condition (N pRRL, Hx pRRL, pRRL-EPAS1PP, pRRL-HIF1αPP, pRRL-EPAS1PPbHLH*, pRRL-HIF1αPPbHLH*) 48 hours after infection is shown. EdU$^+$ nuclei are shown in magenta and nuclei were visualized by DAPI staining. Bar: 100 µm. B, Percentage of EdU$^+$ cells/field in 3-4 independent experiments (10 fields were quantified per experimental condition and each symbol corresponds to the mean value of one experiment) 48 hours after infection. Statistical significance was determined by one-way ANOVA using Tukey's post-test (*$P < .05$, **$P < .01$, ***$P < .001$). C, A representative plot of EdU-Alexa 647 vs DNA content propidium iodide (PI) of each experimental condition 48 hours after infection. Percentage of cells in G_0/G_1, S, and G_2/M phases of the cell cycle is shown inside the corresponding gating regions (magenta lines). D, Percentage of cells in G_0/G_1, S, and G_2/M phases quantified by FACS for each experimental condition 48 hours after infection. Symbols correspond to the value of independent experiments and bars represent the mean of 3-4 independent experiments. Statistical significance was determined by two-way ANOVA using Tukey's post-test (*$P < .05$, **$P < .01$)
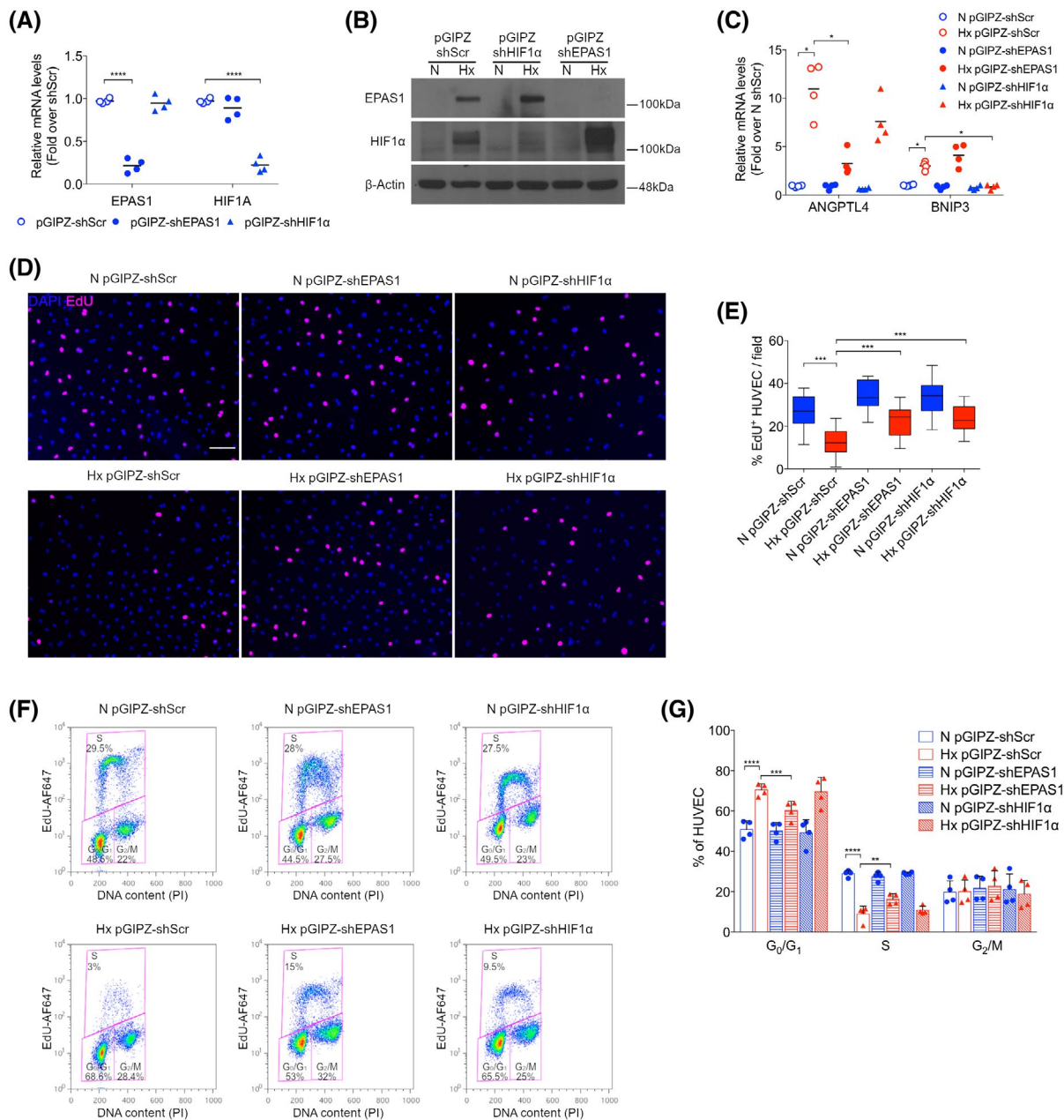
FIGURE 4 Hypoxia-Inducible Factors are required to withdraw HUVEC from S-phase entry in hypoxic conditions. Exponentially growing asynchronous HUVEC were transduced with lentivirus for the expression of shRNAs to specifically silence EPAS1 (pGIPZ-shEPAS1) or HIF1A (pGIPZ-shHIF1α) and a scramble, non-silencing shRNA, was used as control (pGIPZ-shScr) in N or Hx. A, Levels of *EPAS1* and *HIF1A* mRNA were determined by qRT-PCR. The graph represents the ratio over scramble shSrc of four independent experiments. Statistical significance was determined by two-way ANOVA using Tukey's post-test (****$P < .0001$). B, HIF1α and EPAS1 protein expression was analyzed by western-blot. C, Levels of *ANGPTL4* and *BNIP3* mRNA in transduced HUVEC were determined by qRT-PCR. The graph represents the ratio over N pGIPZ-shSrc of four independent experiments. Statistical significance was determined by one-way ANOVA using Tukey's post-test (*$P < .05$). Transduced HUVEC were pulse labeled with EdU to quantify the percentage of S-phase cells by microscopy (D-E) or FACS (F-G) 72 hours after lentiviral infection. D, A representative microscopy image of each experimental condition (pGIPZ-shScr, pGIPZ-shEPAS1 and pGIPZ-shHIF1α) in N or Hx is shown. EdU$^+$ nuclei are shown in magenta and nuclei were visualized by DAPI staining. Bar: 100 μm. E, Box plot of percentage EdU$^+$ cells/field for each experimental condition. Each box represents the mean of two independent experiments (10 fields/experiment) Statistical significance was determined by one-way ANOVA using Tukey's post-test (***$P < .001$). F, A representative plot of EdU-Alexa 647 vs DNA content propidium iodide (PI) for each experimental condition (pGIPZ-shScr, pGIPZ-shEPAS1 and pGIPZ-shHIF1α) in N or Hx conditions is shown. Percentage of cells in G_0/G_1, S, and G_2/M phases of the cell cycle is shown inside the corresponding gating regions (magenta lines). G, Percentage of cells in G_0/G_1, S, and G_2/M phases quantified by FACS for each experimental condition 48 hours after infection. Symbols correspond to the value of independent experiments and bars represent the mean of four independent experiments. Statistical significance was determined by two-way ANOVA using Tukey's post-test (**$P < .01$, ***$P < .001$, ****$P < .0001$)
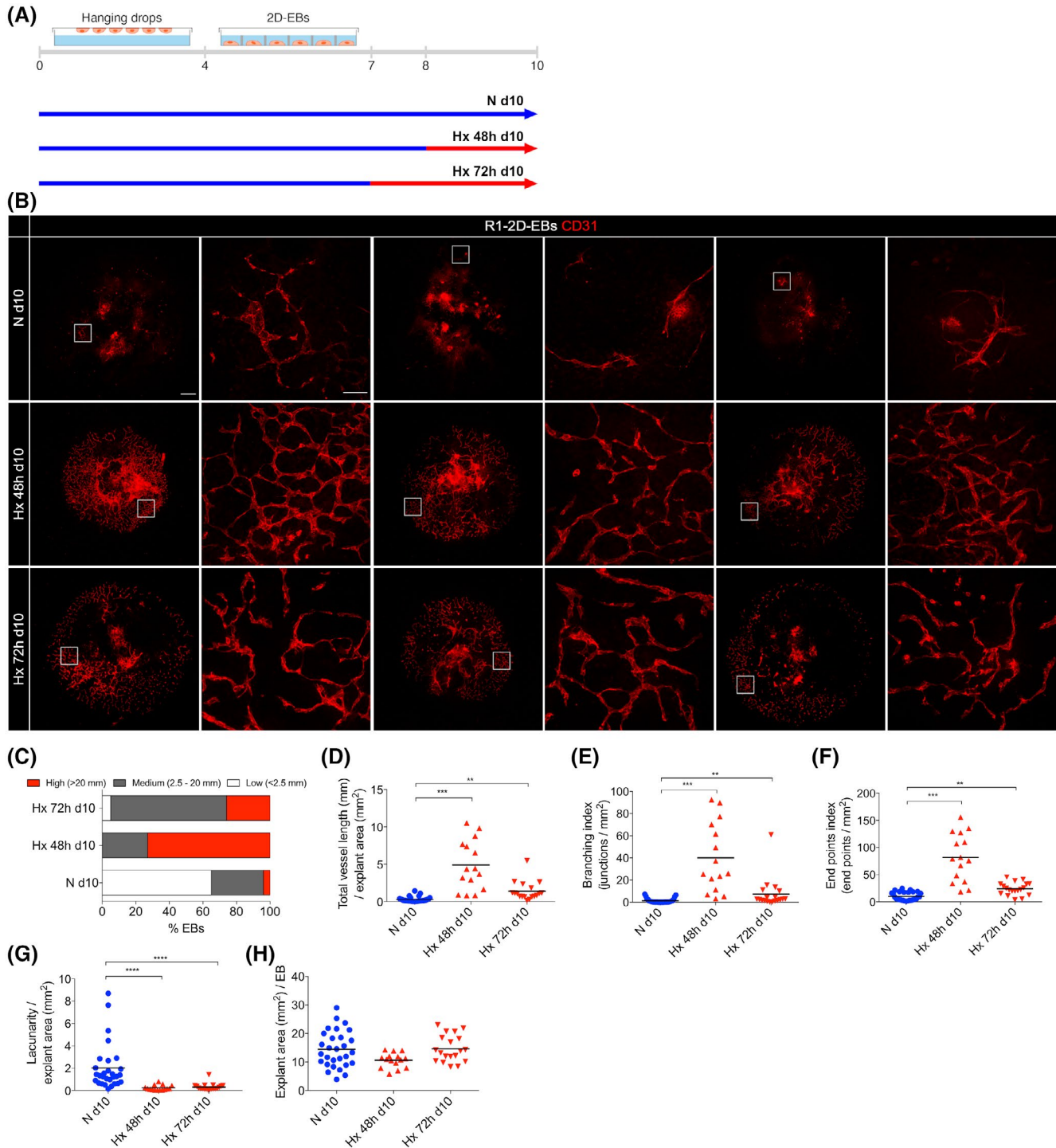
FIGURE 5 Hypoxia induces angiogenesis in 2D Embryoid Bodies derived from R1 mouse Embryonic Stem Cells. A, Scheme of the experimental design. EBs generated from R1 mESCs were differentiated in 2D conditions (R1-2D-EBs) in N and stimulated with Hx during the last 48 hours (Hx 48 hours d10; n = 17 EBs) or 72 hours (Hx 72 hours d10; n = 18 EBs) of a total of 10 days of in vitro differentiation. Control EBs were differentiated in normoxic conditions for 10 days (N d10). Vascular structures were visualized by immunostaining using anti-CD31. B, CD31 staining (red) of three representative EBs of each experimental condition (N d10, Hx 48 hours d10, and Hx 72 hours d10) is shown. Bar: 500 μm. A high-magnification image is shown on the right (the magnified area is indicated by a rectangle in the corresponding EB image). Bar: 80 μm. C, Angiogenesis was quantified using AngioTool analysis software and the percentage of EBs with low (<2.5 mm length, white), medium (2.5-20 mm length, grey) or high (>20 mm length, red) angiogenesis is represented for each experimental condition. A Chi-square analysis showed that the distribution of vessel length was significantly different among conditions (χ^2_4 = 209.9, P < .0001). D-H, AngioTool parameters. Each symbol corresponds to one EB. D, Total vessel length (mm)/explant area (mm^2). E, Branching index (junctions/mm^2). F, End point index (end points/mm^2). G, Lacunarity/explant area (mm^2). H, Explant area (mm^2)/EB. D-H, Statistical significance was determined by one-way ANOVA using Kruskal-Wallis post-test (**P < .01, ***P < .001, ****P < .0001)

determined by the AngioTool software[28] quantitative analysis (Figure 5C). Figure 5D-F shows that hypoxic stimulation significantly augmented total vessel length and complexity of the vascular structures measured by the branching index and end points index. Additionally, lacunarity (opposite to vascular length; and a suitable parameter to detect alterations in the level of organization of a vascular network) was significantly reduced by hypoxia (Figure 5G). Hypoxia treatment did not significantly alter the size of R1-2D-EBs compared to normoxic conditions (Figure 5H).

We next explored whether hypoxia affected EdU incorporation in mature ECs assembled into organized vascular structures in the R1-2D-EBs. To this end, we acquired confocal microscopy images of peripheral vascular structures in the EBs. Taking into account the cellular complexity of the 2D-EBs (including endothelial and non-endothelial cells), we developed a macro that allowed a reliable semi-automatic quantification of EC proliferation in vascular structures at higher cellular resolution based on the combination of a membrane (CD31) and a nuclear (ERG) endothelial-specific marker and the automatic counting of ERG positive nuclei, followed by manual quantification of EdU using ImageJ tools (Supplemental Figure S1A-C). The triple staining EdU-CD31-ERG in four representative images for each experimental condition (N d10, Hx 48hours d10, and Hx 72hours d10) is shown in Figure 6A. The percentage of ECs in S-phase was significantly reduced in vascular structures in the periphery of the EBs maintained 48 or 72 hours in hypoxia compared to normoxia (48 hours Hx 13.9 ± 2.7 vs N 19.9% ± 5.3%; 72 hours Hx 10.2% ± 5.3% vs N 19.9% ± 5.3%) (Figure 6B). Quantification of angiogenesis by AngioTool software analysis of microscopy fields of peripheral structures confirmed that hypoxia increased total vessel length and complexity of the vascular structures measured by the average number of branching points and number of end points (Figure 6C-F).

Additionally, we quantified EdU incorporation in microscopy fields of internal vascular structures in R1-2D-EBs and confirmed that hypoxia also reduced the percentage of S-phase ECs (Supplemental Figure S3A,B) and increased angiogenesis (Supplemental Figure S3C-F).

Taking advantage of the nuclear endothelial-specific marker ERG, we interrogated whether increased angiogenesis observed in the EBs exposed to hypoxia was associated with a change in the total number of ECs per field and the number of ECs per unit of length. Paradoxically, with respect to the observed reduced percentage of S-phase ECs in vascular structures in hypoxia, we found a concomitant increase in the total number of ECs per field in EBs treated with the hypoxic stimulus compared to EBs in normoxia (Hx 48 hours d10 131.1 ± 54.4; Hx 72 hours d10 145.3 ± 53.3; N d10 41.3 ± 26.4) (Figure 6G and Supplemental Figure S3G). However, the number of ECs per unit length remained

constant (Hx 48 hours d10 25.9 ± 3.1; Hx 72 hours d10: 35.7 ± 7.1; N d10 25.0 ± 8.3) (Figure 6H and Supplemental Figure S3H).

We confirmed these results in an independent mESC line (E14TG2a). Although E14TG2a-2D-EBs displayed higher basal angiogenesis in normoxia than R1-2D-EBs, we consistently observed a statistically significant increase in total vessel length and the complexity of the vascular network in the periphery of E14TG2a-2D-EBs (Supplemental Figure S4). Hypoxia also decreased the percentage of S-phase ECs in vascular structures of the periphery of the E14TG2a-2D-EBs (Supplemental Figure S5A,B), while the total number of ECs per field was simultaneously increased (Supplemental Figure S5G), leaving unchanged the number of ECs per unit length (Supplemental Figure S5H).

Quantification by flow cytometry of R1-2D-EBs differentiated 10 days confirmed that a hypoxia treatment in the last 48 hours significantly increased the percentage of differentiated VE-cadherin (CD144) positive ECs (Figure 7A,B). In addition, hypoxia reduced the percentage of S-phase cells in both the VE-cadherin positive (Hx: 11.7 ± 5.4 vs N: 27.4 ± 6.2) (Figure 7C,D) and VE-cadherin negative populations (Hx: 13.6 ± 6.4 vs N: 26.6 ± 5.4) (Figure 7E,F) and significantly increased the percentage of cells in the G_0/G_1 phase in both the VE-cadherin positive (Hx: 77.5 ± 3.2 vs N: 63.9 ± 5.8) and VE-cadherin negative populations (Hx: 77.9 ± 4.9 vs N: 68.6 ± 5.2) (Figure 7D,F); thus, indicating that cell cycle arrest is imposed by hypoxia independent of the differentiation status of the cells in the EB. Combined, these observations support that hypoxia is integrating cell cycle arrest and induction of differentiation of endothelial progenitor cells to increase angiogenesis in the EBs.

Finally, we explored the effect of hypoxia on EC proliferation during the three-dimensional differentiation of EBs generated from an iPS cell line (iPSC-3D-EBs).[40] In the experimental conditions of the 3D model, endothelial differentiation is highly efficient and all the cells sprouting from the core of the EBs stained positive for Isolectin B4 (IB4; Figure 8) and other EC markers (data not shown). The outline of the experiment is summarized in Figure 8A. ECs sprouts protruding from the central core of the EBs were observed from day 5 in 3D normoxic EBs (data not shown). A hypoxic treatment in the last 72 hours or 96 hours of 10 days of differentiation, significantly increased sprouting angiogenesis compared to normoxic EBs (Figure 8B-G: increased explant area, total vessel length, total number of branching points, total number of end points, total number of ECs); while the number of ECs per unit length remained unchanged (Figure 8H). However, in the 3D model hypoxia did not significantly alter the complexity of the vascular network (branching index (junctions/mm^2) and end points index (end points/mm^2) (data not shown)). In agreement with the results obtained in 2D-EBs, quantification of EdU positive ECs in iPSC-3D-EBs revealed a significant
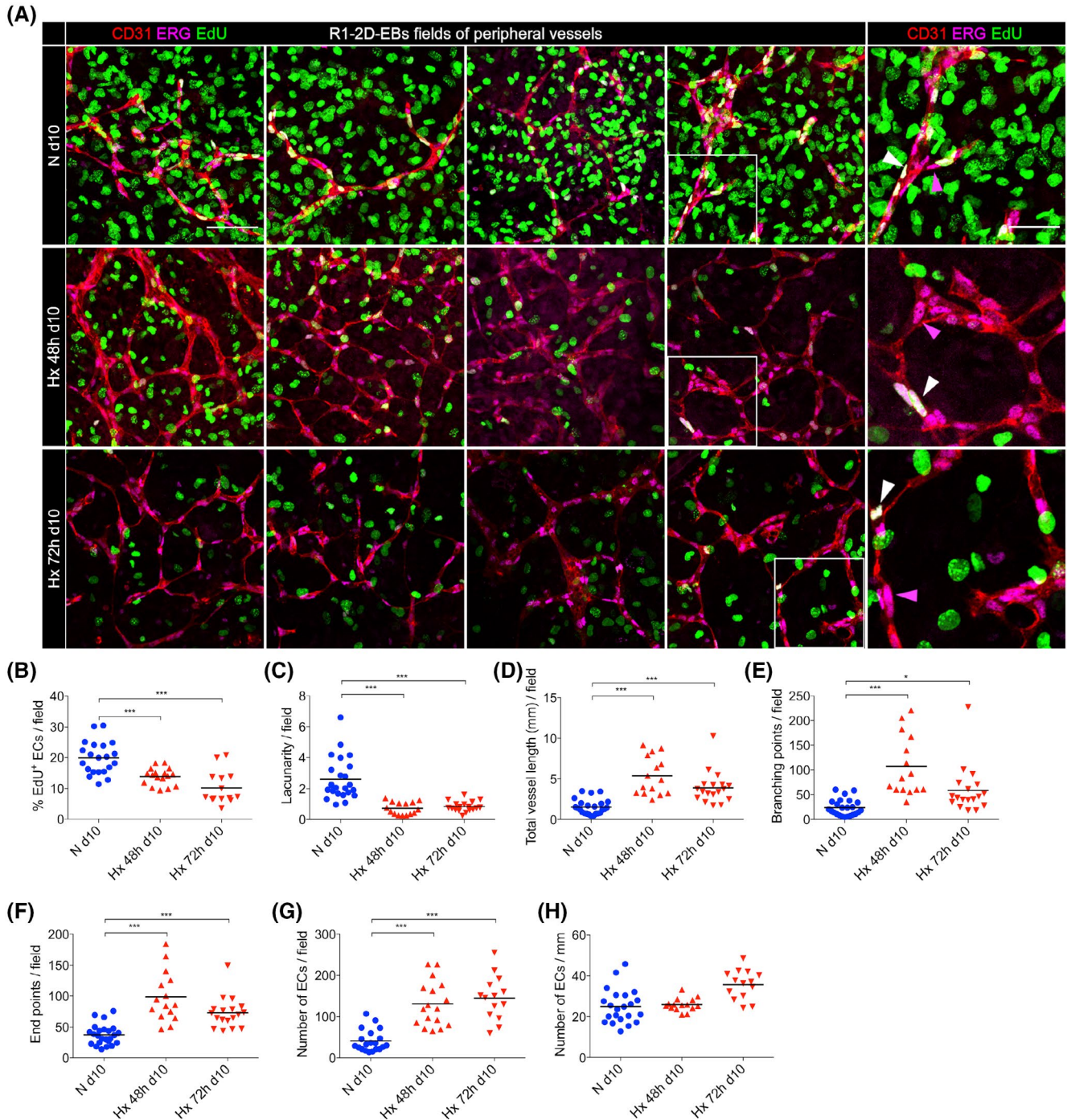
FIGURE 6 Hypoxia decreases the percentage of S-phase endothelial cells in peripheral vascular structures of R1-2D-Embryoid Bodies. EBs generated from R1 mESCs were 2D differentiated (R1-2D-EBs) in N and stimulated with Hx during the last 48 hours (Hx 48 hours d10; n = 17 EBs) or 72 hours (Hx 72 hours d10; n = 18 EBs) of a total of 10 days of in vitro differentiation. Control EBs were differentiated in normoxic conditions for 10 days. EBs were pulse labeled with EdU during the last 3 hours. A, A representative image of peripheral vascular structures of each experimental condition (N d10, Hx 48 hours d10, and Hx 72 hours d10) is shown. Vascular structures were visualized by double immunostaining using anti-CD31 (red) and anti-ERG (magenta)-specific antibodies. S-phase cells were visualized by EdU incorporation (green). Bar: 80 μm. High-magnification images are shown on the right and EdU$^-$ nuclei (magenta triangles) and EdU$^+$ nuclei (white triangles) are indicated. Bar: 50 μm. B-H, Each symbol represents the mean value per EB (5-10 fields/EB). B, Percentage of EdU$^+$ ECs in peripheral vascular structures. Statistical significance was determined by one-way ANOVA using Dunnett's post-test (***$P < .001$). C-F, AngioTool parameters. C, Lacunarity/ field. D, Total vessel length (mm)/field. E, Branching points/field. F, End points/field. (G-H) Number of ECs was determined by automatic counting of ERG$^+$ nuclei on a CD31$^+$-ERG$^+$ mask. G, Number of ECs/field. H, Number of ECs/mm. C-H, Statistical significance was determined by one-way ANOVA using Kruskal-Wallis post-test (*$P < .05$, ***$P < .001$)
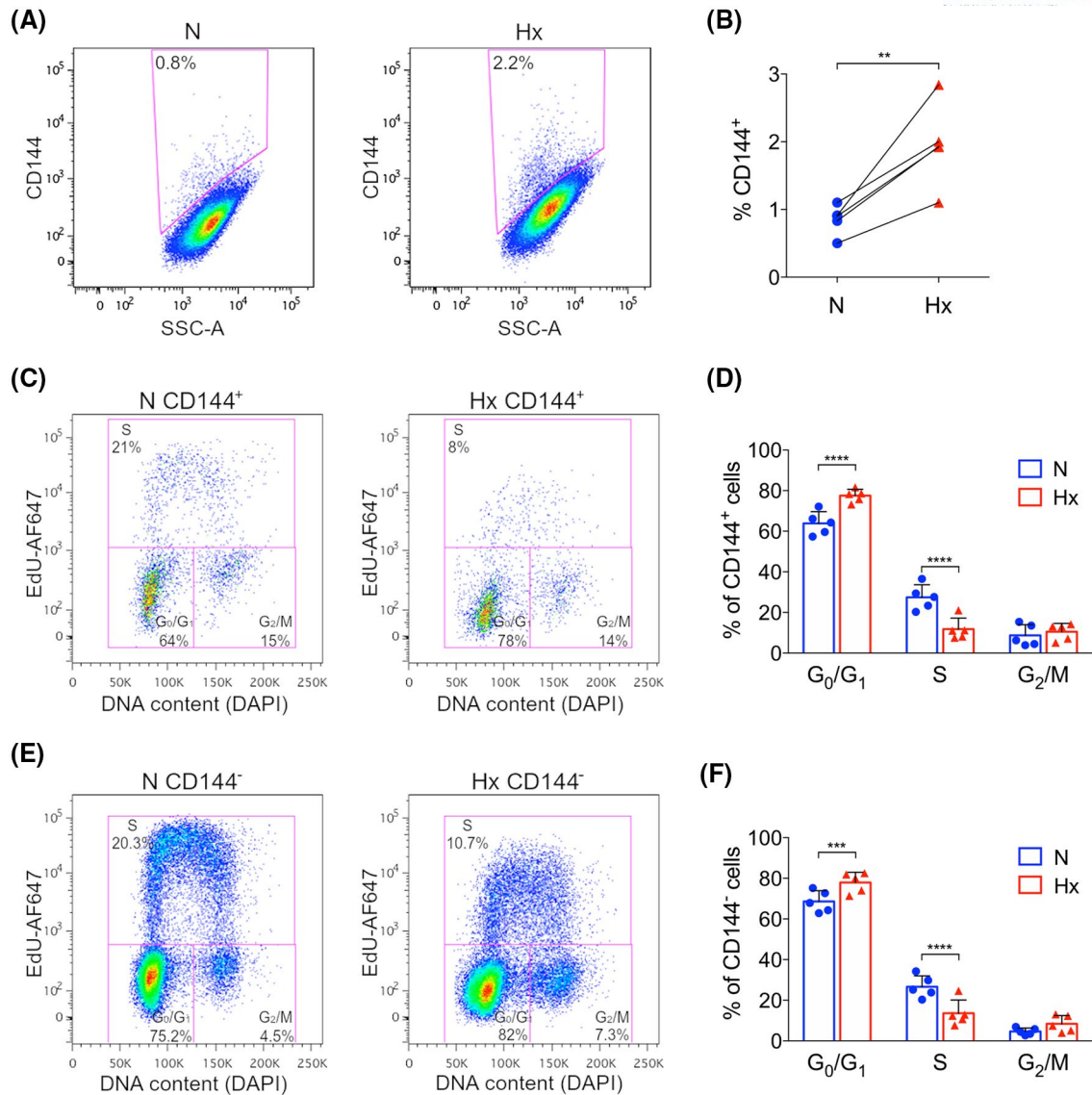
FIGURE 7 Flow cytometry analysis of the effect of hypoxia on S-phase entry in R1-2D-Embryoid Bodies. 2D-EBs generated from R1 mESCs were differentiated in N and stimulated with Hx during the last 48 hours of a total of 10 days of in vitro differentiation. Control EBs were differentiated in normoxic conditions for 10 days (N d10). EBs were pulse labeled with EdU during the last 1 hour and analyzed by flow cytometry for CD144 (VE-cadherin) expression and EdU labelling. A, Representative plot of the percentage of $CD144^+$ cells in EBs in N (left plot) and Hx (right plot) is shown. The region of CD144-labeled cells is indicated by the magenta line and the percentage of $CD144^+$ cells is shown inside. B, The percentage of $CD144^+$ cells was determined by FACS in N (blue circles) or Hx (red triangles) in five independent experiments. Results from each independent experiment are linked by a line. Statistical significance was determined by paired sample Student's t-test (**$P < .01$). C, Representative plot of EdU-Alexa 647 vs DNA content DAPI in the $CD144^+$ population in EBs from N (left plot) or Hx (right plot). The percentage of cells in G_0/G_1, S, and G_2/M phases of the cell cycle is shown inside the corresponding gating regions (magenta lines). D, Percentage of $CD144^+$ cells in G_0/G_1, S, and G_2/M phases quantified by FACS. Symbols correspond to the value of independent experiments and bars represent the mean of five independent experiments. E, Representative plot of EdU-Alexa 647 vs DNA content DAPI in the $CD144^-$ population in EBs from N (left plot) or Hx (right plot). Percentage of cells in G_0/G_1, S, and G_2/M phases of the cell cycle is shown inside the corresponding gating regions (magenta lines). F, Percentage of $CD144^-$ cells in G_0/G_1, S, and G_2/M phases quantified by FACS. Symbols correspond to the value of independent experiments and bars represent the mean of five independent experiments. D and F, Statistical significance was determined by two-way ANOVA using Sidak's post-test (***$P < .001$, ****$P < .0001$)

decrease in the percentage S-phase ECs in hypoxic conditions (Hx 72 hours d10 44.2 ± 10.7; Hx 96 hours d10 47.2 ± 10.2; N d10 72.5 ± 9.4) (Figure 8I).

Thus, globally, our results in a physiologically relevant model showed that hypoxia triggered an autoregulatory cell cycle exit that is integrated with enhanced differentiation of
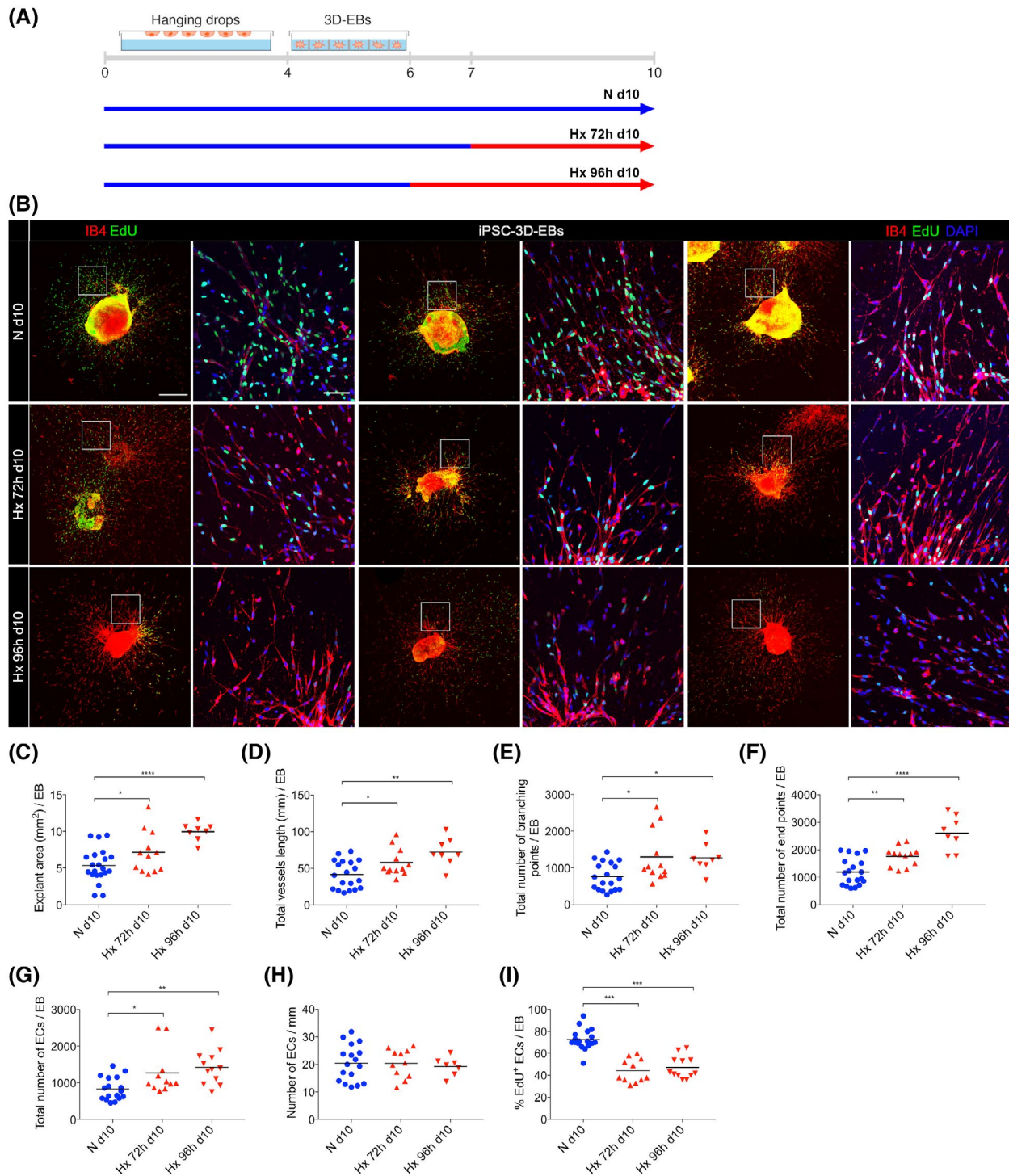
FIGURE 8 Hypoxia induces angiogenesis and decreases the percentage S-phase endothelial cells in vascular structures in iPSC-3D-Embryoid Bodies. A, Scheme of the experimental design. EBs generated from iPSC were differentiated in 3D conditions (iPSC-3D-EBs) in N and stimulated with Hx during the last 72 hours (Hx 72 hours d10; n = 12 EBs) or 96 hours (Hx 96 hours d10; n = 12 EBs) of a total of 10 days of in vitro differentiation. Control EBs were differentiated in normoxic conditions for 10 days (N d10; n = 21). B, Vascular structures were visualized by Isolectin B4 staining (IB4) (Red) and S-phase cells by EdU incorporation (green). Three representative EBs per experimental condition are shown. Bar: 500 μm. A high-magnification image is shown on the right (the magnified area is indicated by a rectangle in the corresponding EB image). Bar: 80 μm. C-F, AngioTool parameters. Each symbol corresponds to one EB. C, Explant area (mm^2)/EB. D, Total vessel length (mm)/EB. E, Total number of branching points/EB. F, Total number of end points/EB. C-F, Statistical significance of AngioTool parameters was determined by one-way ANOVA using Holm-Sidak's post-test (*$P < .05$, **$P < .01$, ****$P < .0001$). G-H, Number of ECs was determined by automatic counting using a DAPI mask. G, Total number of ECs in vascular structures/EB. H, Average number of ECs/mm. I, Percentage of EdU$^+$ ECs/EB. G-I, Statistical significance was determined by one-way ANOVA using Holm-Sidak's post-test (*$P < .05$, **$P < .01$, ***$P < .001$)

progenitor cells to increase the extension and complexity of a pre-existing vascular network.

4 | DISCUSSION

The formation of new blood vessels for tissue homeostasis requires a finely tuned temporal and spatial control of the biology of ECs. Among the cellular responses integrated during angiogenesis, cell growth, and division stand pivotal for the generation of a fully functional vascular plexus.[16-18,20] However, the molecular underpinnings of EC proliferation during angiogenesis remain scarcely known.[41,42] Hypoxia, at the crossroad of physiology and pathology, is a major stimulus of angiogenesis, but how ECs respond to hypoxia still remains poorly understood. Here, we aimed to get further insight into the adaptive response of ECs to hypoxia by exploring in depth the impact of low oxygen on endothelial cell cycle dynamics during angiogenesis. To this end, we first made use of data from our previous global analysis intended to study the transcriptional regulation of gene expression by hypoxia in HUVEC using affinity capture of 4sU-labeled transcripts followed by high-throughput sequencing.[31] A subsequent Gene Ontology analysis of the data from this experiment allowed us to identify that biological categories related to cell cycle regulation and DNA replication, were significantly enriched in the genes downregulated in HUVEC by 8 hours exposure to hypoxia. Thus, a response of ECs to cope with low oxygen involves readjusting their cell division cycle dynamics. The gene expression changes observed in our study indicate that the G1/S cell cycle check point and initiation of DNA replication are blocked very early in ECs exposed to hypoxia. Fundamental regulators of G1/S transition like *CCND1*, *CDC25A*, and several E2F family members were downregulated; while *CDK* inhibitors like *INK4*, *KIP1,2* were upregulated, in HUVEC exposed to hypoxic conditions (Figure 1C,D), suggesting a coordinated transcriptional response that hinders cell cycle progression. Also, a large number of genes of the basic machinery for the control of initiation of DNA replication (*ORC* and *MCM* gene families), together with *CDC6* and *CDC45*, were repressed (Figure 1C). Paradoxically, this early anti-proliferative signature is concomitant with the upregulation of a number of genes implicated in mounting an angiogenic response (Figure 1A,B). Previous transcriptomic analysis in ECs also showed the downregulation of genes related to cell proliferation.[43-45] However, none of those studies provided a functional validation in ECs during angiogenesis.

In agreement with the anti-proliferative signature, we found that hypoxia significantly decreased the percentage of HUVEC in the S-phase of the cell cycle and slowed-down proliferation rate (Figure 2). Hypoxia has been shown to inhibit the proliferation of numerous cell types including fibroblasts,[46,47] stem cells,[48] lymphocytes,[47] keratinocytes[49], and several cancer cell lines.[50-52] Although, the general trend is the inhibition of proliferation by hypoxia, there are a number of exceptions regarding some cell types and tissue-specific contexts. For example, hypoxia induces the proliferation of bronchial club epithelial cells,[53] Human aortic cells[54] and type H endothelial cells during bone formation.[55] Thus, distinct types of endothelial cells could behave differently in response to hypoxia to accomplish specific cellular responses. Although it has not been explored yet, tip endothelial cells must also respond differently to hypoxia than stalk endothelial cells; as tips cells at the leading edge of the sprout, face lower oxygen tensions and have to remain quiescent to allow for migration and guidance of the new vessels, while stalk cells must proliferate to increase vessel size.[42,56] A deeper understanding of the mechanisms that finely tune endothelial cell proliferation during the remodeling of the vasculature in response to hypoxia will be relevant for a successful therapeutic intervention in pathological contexts.

We next investigated the role of HIF in the control of EC proliferation. In agreement with the fact that EPAS1 is the most abundant isoform in HUVEC and it is responsible for the majority of the transcriptional activity,[31] we found that *EPAS1* is predominantly involved in the adaptive reprogramming of the cell cycle of HUVEC in hypoxia. Expression of the active EPAS1PP mutant in normoxia (Figure 3) decreased the percentage of HUVEC in S-phase of the cell cycle; while the interference of *EPAS1* by shRNA abrogated the anti-proliferative response of HUVEC to hypoxia (Figure 4). Notwithstanding, HIF1α contributes to the same biological response, as the expression of active HIF1αPP mutant or interference of *HIF1A* not always reached statistical significance (Figures 3 and 4). Additionally, we found that mutation of the bHLH domain abrogated the effect of HIF mutants on S-phase (Figures 3 and 4). Thus, our results demonstrate that decreased EC proliferation by hypoxia is mainly an EPAS1-driven response that requires transcriptional activity.

Previous studies have explored functional differences between HIF1α and EPAS1. In renal cell carcinoma cells EPAS1 stimulated cell proliferation through MYC activation[50]; while HIF1α induced cell cycle arrest in colon carcinoma cells by counteracting MYC.[52] In another study in mouse embryonic fibroblasts and splenic B lymphocytes deletion of *HIF1A* abolished hypoxia-induced cell cycle arrest in a p53-independent manner.[47] More recently, the functional impact of the conditional deletion of *EPAS1* or *HIF1A* in ECs has been addressed.[57] *EPAS1* deletion resulted in increased vessel formation in vivo (higher vessel density and branching, but poor perfusion and low pericyte coverage), likely mediated by its downstream effect on DLL4/NOTCH1 in ECs,[57] while *HIF1A* deletion resulted in decreased vessel formation in vivo (lower vessel density, branching, perfusion, and pericyte coverage).[57,58] These results support that EPAS1 is a major brake

to EC division and that integration of the regulatory action of both HIF1α and EPAS1 is required to adequately balance proliferation during angiogenesis for the formation of a fully functional vascular plexus. However, although our results supported a role of EPAS1 as a negative regulator of EC proliferation in hypoxia, they did not support an antagonistic role of HIF1α. In addition, it is known that HIF1α and EPAS1 respond differently to hypoxia. While HIF1α has a rapid response to acute hypoxia, EPAS1 has a more long-term response to low oxygen levels.[59] As angiogenesis is a highly energy demanding process, it is reasonable to be only triggered by chronic hypoxia and thus mainly driven by EPAS1.

Regarding the role of the Notch pathway, our transcriptome analysis and qRT-PCR validation showed that *DLL4* is upregulated by hypoxia in HUVEC (data not shown); being a candidate to mediate cell growth arrest imposed by EPAS1 in ECs. Another candidate is *MYC*; a fundamental driver of proliferation, commonly altered in a variety of cancers that could be indirectly inhibited in HUVEC in hypoxia by the upregulation of its inhibitory member *MXI1*.[31] MYC has been recently demonstrated to be a critical switch for the activation of quiescent ECs; being FOXO1 regulation by VEGFA the mechanism involved in allowing MYC activation of EC metabolism and growth.[41,60]

In order to get insight into the regulation of EC proliferation by hypoxia during blood vessel formation we employed the EB model; an ESC-derived model that faithfully recapitulates vasculogenesis and angiogenesis.[37] It has been previously shown that 48 hours hypoxic treatment during EBs formation (from day 3 to day 5) accelerated vascular lineage differentiation and angiogenesis at day 14.[38] Taking into account this result we set up our experimental design to interrogate the effect of reduced oxygen tension in the proliferation dynamics of highly organized vascular structures in late-stage differentiated EBs (day 10). Quantitative analysis of EdU incorporation by confocal microcopy in 2D-EBs generated from two different mESC lines (R1 and E14TG2a) demonstrated that hypoxia reduced the percentage of S-phase ECs in peripheral (Figure 6 and Supplemental Figure S5) and internal (Supplemental Figure S3) vascular structures. Paradoxically, reduced proliferation in hypoxic conditions was concomitant with an increased number of ECs (Figure 6G and Supplemental Figure S5G) and increased angiogenesis (Figures 5 and 6 and Supplemental Figures S3-S5).

Analysis by flow cytometry of 2D-EBs demonstrated that in EBs differentiated 10 days, stimulation by hypoxia in the last 48 hours increased the percentage of differentiated VE-cadherin positive cells (Figure 7A,B). In addition, hypoxia significantly decreased S-phase in both the VE-cadherin positive and VE-cadherin negative cells in the EBs (Figure 7C-F). These results support that cell cycle arrest is a primary response to hypoxia independent of the degree of differentiation.

Our results in the 3D-EB model confirmed that hypoxia reduced the percentage of ECs in S-phase (Figure 8B,I) but increased the total number of ECs per EB (Figure 8G). This increase in the total number of ECs per EB is in agreement with the observed increase in 3D-sprouting angiogenesis (Figure 8C-F).

Thus, in the EB model, the anti-proliferative response imposed by hypoxia in mature ECs is most likely compensated by induction of progenitor differentiation which is favored by cell cycle exit.[61,62] Although counterintuitive for the mechanism of angiogenesis, slowing-down of EC proliferation could streamline the making of new vessels, as it could be beneficial for optimum network formation and vessel maturation. EPAS1 could have a prominent role in restricting EC proliferation in vivo, as its stabilization by endothelial deletion of *PHD2* (*EGLN1*) promoted a growth-arrested phenotype (phalanx ECs) and the normalization of tumor vessels[63]; while the endothelial deletion of *EPAS1* increased vessel density, but lead to an immature and poorly functional vasculature.[22] Moreover, in a mouse model of conditional inducible expression of the stabilized mutant *HIF1αPP* in keratinocytes, angiogenesis is associated with an early hyper-proliferative response that is followed by cell growth arrest.[64] Although an early and transient hyper-proliferative response to hypoxia could potentially explain our findings in the EB model, we disregarded this possibility based on our transcriptomic analysis in HUVEC which showed that the anti-proliferative gene expression signature is present at 8 hours and was maintained over time (latest experimental time point 16 hours, data not shown). In future experiments in the EB model, it would be relevant to use the constitutively active mutant EPAS1PP and the loss of function mutant EPAS1PPbHLH* to explore whether inhibition of EC proliferation is a cell-autonomous response mediated by the transcriptional activity of EPAS1. Additionally, the use of genome-wide CRISPR functional approaches in cell lines could be instrumental in the identification of critical targets for endothelial cell growth arrest in hypoxia. Although the molecular underpinnings of the particular mechanism involved remain elusive; their knowledge would be relevant for the design of improved strategies aimed to suppress angiogenesis in pathological contexts where hypoxia is a central driver of neovascularization.

ACKNOWLEDGMENTS

CONFLICT OF INTEREST

The authors decleare they have no conflict of interest.

AUTHOR CONTRIBUTIONS

B. Jiménez, L. del Peso, and B. Acosta-Iborra designed the experiments; B. Acosta-Iborra, B. Jiménez, M. Tiana, L. Maeso-Alonso, R. Hernández-Sierra, G. Herranz, A. Santamaria, C. Rey and R. Luna performed experiments; B. Acosta-Iborra, B. Jiménez, L. Maeso-Alonso, G. Herranz, and A. Santamaria acquired and quantified microscopy images; B. Acosta-Iborra, M. Tiana., L. Maeso-Alonso, L. Puente-Santamaria[1], M. M. Marques, MC Marin, L. del Peso, and B. Jiménez interpreted the data and provided expert advice on methods; B. Jiménez wrote the paper.

REFERENCES

1. Semenza GL. Hypoxia-inducible factors in physiology and medicine. *Cell*. 2012;148:399-408.

2. Tian H, McKnight SL, Russell DW. Endothelial PAS domain protein 1 (EPAS1), a transcription factor selectively expressed in endothelial cells. *Genes Dev*. 1997;11:72-82.

3. Ema M, Taya S, Yokotani N, Sogawa K, Matsuda Y, Fujii-Kuriyama Y. A novel bHLH-PAS factor with close sequence similarity to hypoxia-inducible factor 1alpha regulates the VEGF expression and is potentially involved in lung and vascular development. *Proc Natl Acad Sci USA*. 1997;94:4273-4278.

4. Hogenesch JB, Chan WK, Jackiw VH, et al Characterization of a subset of the basic-helix-loop-helix-PAS superfamily that interacts with components of the dioxin signaling pathway. *J Biol Chem*. 1997;272:8581-8593.

5. Wiesener MS, Turley H, Allen WE, et al Induction of endothelial PAS domain protein-1 by hypoxia: characterization and comparison with hypoxia-inducible factor-1alpha. *Blood*. 1998;92:2260-2268.

6. Kaelin WGJ, Ratcliffe PJ. Oxygen sensing by metazoans: the central role of the HIF hydroxylase pathway. *Mol Cell*. 2008;30:393-402.

7. Hu C-J, Wang L-Y, Chodosh LA, Keith B, Simon MC. Differential roles of hypoxia-inducible factor 1alpha (HIF-1alpha) and HIF-2alpha in hypoxic gene regulation. *Mol Cell Biol*. 2003;23:9361-9374.

8. Salama R, Masson N, Simpson P, et al Heterogeneous effects of direct hypoxia pathway activation in kidney cancer. *PLoS ONE*. 2015;10:e0134645.

9. Semenza GL. Oxygen sensing, hypoxia-inducible factors, and disease pathophysiology. *Annu Rev Pathol Mech Dis*. 2014;9:47-71.

10. Schito L, Semenza GL. Hypoxia-inducible factors: master regulators of cancer progression. *Trends Cancer*. 2016;2:758-770.

11. Rey S, Schito L, Wouters BG, Eliasof S, Kerbel RS. Targeting hypoxia-inducible factors for antiangiogenic cancer therapy. *Trends Cancer*. 2017;3:529-541.

12. Germain S, Monnot C, Muller L, Eichmann A. Hypoxia-driven angiogenesis: role of tip cells and extracellular matrix scaffolding. *Curr Opin Hematol*. 2010;17:245-251.

13. Casazza A, Di Conza G, Wenes M, Finisguerra V, Deschoemaeker S, Mazzone M. Tumor stroma: a complexity dictated by the hypoxic tumor microenvironment. *Oncogene*. 2013;33:1743.

14. Jain RK. Antiangiogenesis strategies revisited: from starving tumors to alleviating hypoxia. *Cancer Cell*. 2014;26:605-622.

15. Wong BW, Marsch E, Treps L, Baes M, Carmeliet P. Endothelial cell metabolism in health and disease: impact of hypoxia. *EMBO J*. 2017;36:2187-2203.

16. Noguera-Troise I, Daly C, Papadopoulos NJ, et al Blockade of Dll4 inhibits tumour growth by promoting non-productive angiogenesis. *Nature*. 2006;444:1032-1037.

17. Fong GH, Rossant J, Gertsenstein M, Breitman ML. Role of the Flt-1 receptor tyrosine kinase in regulating the assembly of vascular endothelium. *Nature*. 1995;376:66-70.

18. Kearney JB, Ambler CA, Monaco K-A, Johnson N, Rapoport RG, Bautch VL. Vascular endothelial growth factor receptor Flt-1 negatively regulates developmental blood vessel formation by modulating endothelial cell division. *Blood*. 2002;99:2397-2407.

19. Serra H, Chivite I, Angulo-Urarte A et al PTEN mediates notch-dependent stalk cell arrest in angiogenesis. *Nat Commun*. 2015;6:7935.

20. Pontes-Quero S, Fernandez-Chacon M, Luo W et al High mitogenic stimulation arrests angiogenesis. *Nat Commun*. 2019;10:2016.

21. Huang H, Vandekeere S, Kalucka J et al Role of glutamine and interlinked asparagine metabolism in vessel formation. *EMBO J*. 2017;36:2334-2352.

22. Skuli N, Liu L, Runge A et al Endothelial deletion of hypoxia-inducible factor-2alpha (HIF-2alpha) alters vascular function and tumor angiogenesis. *Blood*. 2009;114:469-477.

23. Centanin L, Dekanty A, Romero N, Irisarri M, Gorr TA, Wappner P. Cell autonomy of HIF effects in Drosophila: tracheal cells sense hypoxia and induce terminal branch sprouting. *Dev Cell*. 2008;14:547-558.

24. Shalaby F, Rossant J, Yamaguchi TP et al Failure of blood-island formation and vasculogenesis in Flk-1-deficient mice. *Nature*. 1995;376:62-66.

25. Kuehn MR, Bradley A, Robertson EJ, Evans MJ. A potential animal model for Lesch-Nyhan syndrome through introduction of HPRT mutations into mice. *Nature*. 1987;326:295-298.

26. Martin-Lopez M, Maeso-Alonso L, Fuertes-Alvarez S et al p73 is required for appropriate BMP-induced mesenchymal-to-epithelial transition during somatic cell reprogramming. *Cell Death Dis*. 2017;8:e3034.

27. Collins TJ. ImageJ for microscopy. *Biotechniques*. 2007;43: S25-S30.

28. Zudaire E, Gambardella L, Kurcz C, Vermeren S. A computational tool for quantitative analysis of vascular networks. *PLoS ONE*. 2011;6:1-12.

29. Gentleman RC, Carey VJ, Bates DM et al Bioconductor: open software development for computational biology and bioinformatics. *Genome Biol*. 2004;5:R80.

30. Robinson MD, McCarthy DJ, Smyth GK. edgeR: a Bioconductor package for differential expression analysis of digital gene expression data. *Bioinformatics*. 2010;26:139-140.

31. Tiana M, Acosta-Iborra B, Puente-Santamaria L et al The SIN3A histone deacetylase complex is required for a complete transcriptional response to hypoxia. *Nucleic Acids Res*. 2018;46:120-133.

32. Yu G, Wang L-G, Han Y, He Q-Y. clusterProfiler: an R package for comparing biological themes among gene clusters. *OMICS*. 2012;16:284-287.

33. Fernandez-Barral A, Orgaz JL, Baquero P et al Regulatory and functional connection of microphthalmia-associated transcription factor and anti-metastatic pigment epithelium derived factor in melanoma. *Neoplasia*. 2014;16:529-542.

34. Kondo K, Klco J, Nakamura E, Lechpammer M, Kaelin WG. Inhibition of HIF is necessary for tumor suppression by the von Hippel-Lindau protein. *Cancer Cell*. 2002;1:237-246.

35. Batie M, Del Peso L, Rocha S. Hypoxia and Chromatin. A focus on transcriptional repression mechanisms. *Biomedicines*. 2018;6:pii:E47.

36. Choudhry H, Harris AL. Advances in hypoxia-inducible factor biology. *Cell Metab*. 2018;27:281-298.

37. Jakobsson L, Kreuger J, Claesson-Welsh L. Building blood vessels – stem cell models in vascular biology. *J Cell Biol*. 2007;177:751-755.

38. Lee SW, Jeong HK, Lee JY et al Hypoxic priming of mESCs accelerates vascular-lineage differentiation through HIF1-mediated inverse regulation of Oct4 and VEGF. *EMBO Mol Med*. 2012;4:924-938.

39. Tsang KM, Hyun JS, Cheng KT et al Embryonic stem cell differentiation to functional arterial endothelial cells through sequential activation of ETV2 and NOTCH1 signaling by HIF1α. *Stem Cell Rep*. 2017;9:796-806.

40. Fernandez-Alonso R, Martin-Lopez M, Gonzalez-Cano L et al p73 is required for endothelial cell differentiation, migration and the formation of vascular networks regulating VEGF and TGFbeta signaling. *Cell Death Differ*. 2015;22:1287-1299.

41. Wilhelm K, Happel K, Eelen G et al FOXO1 couples metabolic activity and growth state in the vascular endothelium. *Nature*. 2016;529:216-220.

42. Potente M, Carmeliet P. The link between angiogenesis and endothelial metabolism. *Annu Rev Physiol*. 2017;79:43-66.

43. Scheurer SB, Rybak JN, Rosli C, Neri D, Elia G. Modulation of gene expression by hypoxia in human umbilical cord vein endothelial cells: a transcriptomic and proteomic study. *Proteomics*. 2004;4:1737-1760.

44. Ning W, Chu TJ, Li CJ, Choi AMK, Peters DG. Genome-wide analysis of the endothelial transcriptome under short-term chronic hypoxia. *Physiol Genomics*. 2004;18:70-78.

45. Peters DG, Ning W, Chu TJ, Li CJ, Choi AMK. Comparative SAGE analysis of the response to hypoxia in human pulmonary and aortic endothelial cells. *Physiol Genomics*. 2006;26:99-108.

46. Gardner LB, Li Q, Park MS, Flanagan WM, Semenza GL, Dang CV. Hypoxia inhibits G1/S transition through regulation of p27 expression. *J Biol Chem*. 2001;276:7919-7926.

47. Goda N, Ryan HE, Khadivi B, McNulty W, Rickert RC, Johnson RS. Hypoxia-inducible factor 1alpha is essential for cell cycle arrest during hypoxia. *Mol Cell Biol*. 2003;23:359-369.

48. Carmeliet P, Dor Y, Herbert JM et al Role of HIF-1alpha in hypoxia-mediated apoptosis, cell proliferation and tumour angiogenesis. *Nature*. 1998;394:485-490.

49. Biswas S, Roy S, Banerjee J et al Hypoxia inducible microRNA 210 attenuates keratinocyte proliferation and impairs closure in a murine model of ischemic wounds. *Proc Natl Acad Sci USA*. 2010;107:6976-6981.

50. Gordan JD, Bertout JA, Hu C-J, Diehl JA, Simon MC. HIF-2alpha promotes hypoxic cell proliferation by enhancing c-myc transcriptional activity. *Cancer Cell*. 2007;11:335-347.

51. Hubbi ME, Kshitiz, Gilkes DM et al A nontranscriptional role for HIF-1alpha as a direct inhibitor of DNA replication. *Sci Signal*. 2013;6:ra10.

52. Koshiji M, Kageyama Y, Pete EA, Horikawa I, Barrett JC, Huang LE. HIF-1alpha induces cell cycle arrest by functionally counteracting Myc. *EMBO J*. 2004;23:1949-1956.

53. Torres-Capelli M, Marsboom G, Li QOY et al Role of Hif2alpha oxygen sensing pathway in bronchial epithelial club cell proliferation. *Sci Rep*. 2016;6:25357.

54. Humar R, Kiefer FN, Berns H, Resink TJ, Battegay EJ. Hypoxia enhances vascular cell proliferation and angiogenesis in vitro via rapamycin (mTOR)-dependent signaling. *FASEB J*. 2002;16:771-780.

55. Kusumbe AP, Ramasamy SK, Adams RH. Coupling of angiogenesis and osteogenesis by a specific vessel subtype in bone. *Nature*. 2014;507:323-328.

56. Draoui N, de Zeeuw P, Carmeliet P. Angiogenesis revisited from a metabolic perspective: role and therapeutic implications of endothelial cell metabolism. *Open Biol*. 2017;7:pii:170219.

57. Skuli N, Majmundar AJ, Krock BL et al Endothelial HIF-2alpha regulates murine pathological angiogenesis and revascularization processes. *J Clin Invest*. 2012;122:1427-1443.

58. Tang N, Wang L, Esko J et al Loss of HIF-1alpha in endothelial cells disrupts a hypoxia-driven VEGF autocrine loop necessary for tumorigenesis. *Cancer Cell*. 2004;6:485-495.

59. Koh MY, Powis G. Passing the baton: the HIF switch. *Trends Biochem Sci*. 2012;37:364-372.

60. Betsholtz C. Vascular biology: transcriptional control of endothelial energy. *Nature*. 2016;529:160-161.

61. Bunce C, Capel B. Cycling in the cell fate landscape. *Curr Top Dev Biol*. 2016;116:153-165.

62. Lim S, Kaldis P. Cdks, cyclins and CKIs: roles beyond cell cycle regulation. *Development*. 2013;140:3079-3093.

63. Mazzone M, Dettori D, de Oliveira RL, et al Heterozygous deficiency of PHD2 restores tumor oxygenation and inhibits metastasis via endothelial normalization. *Cell*. 2009;136:839-851.

64. Oladipupo SS, Hu S, Santeford AC et al Conditional HIF-1 induction produces multistage neovascularization with stage-specific sensitivity to VEGFR inhibitors and myeloid cell independence. *Blood*. 2011;117:4142-4153.

SUPPORTING INFORMATION

Additional supporting information may be found online in the Supporting Information section.

How to cite this article: Acosta-Iborra B, Tiana M, Maeso-Alonso L, et al. Hypoxia compensates cell cycle arrest with progenitor differentiation during angiogenesis. *The FASEB Journal*. 2020;34:6654–6674. https://doi.org/10.1096/fj.201903082R